Progress in Polymer Science 39 (2014) 862–890

Contents lists available at ScienceDirect

Progress in Polymer Science

journal homepage: www.elsevier.com/locate/ppolysci

Advances in three-dimensional nanofibrous macrostructures via electrospinning

B. Sun[a,b], Y.Z. Long[a,b,c,*], H.D. Zhang[a,b], M.M. Li[a,d], J.L. Duvail[e], X.Y. Jiang[d,**], H.L. Yin[f]

[a] College of Physics, Qingdao University, Qingdao 266071, China
[b] Key Laboratory of Photonics Materials & Technology in Universities of Shandong (Qingdao University), Qingdao 266071, China
[c] State Key Laboratory Cultivation Base of New Fiber Materials & Modern Textile, Qingdao University, Qingdao 266071, China
[d] National Center for NanoScience and Technology, Beijing 100190, China
[e] Institut des Matériaux Jean Rouxel, CNRS, Université de Nantes, F-44322 Nantes, France
[f] Department of Osteology, No. 401 Hospital of P. L. A., Qingdao 266071, China

ARTICLE INFO

Article history:
Received 26 October 2012
Received in revised form 27 May 2013
Accepted 31 May 2013
Available online 10 June 2013

Keywords:
Electrospinning
3D nanofibrous macrostructures
Tissue engineering
Energy harvesting and storage
Filtration

ABSTRACT

Compared with other nanofiber fabrication processes, electrospinning is versatile and superior in production and construction of ordered or more complex nanofibrous assemblies. Besides traditional two-dimensional (2D) nanofibrous structures, electrospinning is powerful in fabrication of three-dimensional (3D) fibrous macrostructures, especially for tissue engineering applications. This article summarizes and reviews recent advances in various promising and cutting-edge electrospinning techniques, including multilayering electrospinning, post-processing after electrospinning, liquid-assisted collection, template-assisted collection, porogen-added electrospinning, and self-assembly. And their formation mechanisms, features, and the challenges of electrospinning have also been discussed. Furthermore, these 3D nanofibrous macrostructures have been demonstrated to have potential applications in tissue engineering, energy harvesting and storage, and filtration.
© 2013 Elsevier Ltd. All rights reserved.

Contents

1. Introduction 863
2. Electrospinning background 864
   2.1. Electrospinning process 865
      2.1.1. Jet initiation and straight elongation 865
      2.1.2. Growth of bending instability and further elongation 866

Abbreviations: 1D, one-dimensional; 2D, two dimensional; 3D, three-dimensional; DPMD, direct polymer melt deposition; DSSC, dye sensitized solar cell; ECM, extracellular matrix; EDC, 1-ethyl-3-(3-dimenthylaminopropyl) carbodiimide hydrochloride; GAG, glycosaminoglycan; HAp, hydroxyapatite; HUVEC, human umbilical vein endothelial cell; μCT, micro-computed tomographic; MTT, mitochondrial metabolic; PAN, polyacrylonitrile; PAMPS, poly(2-acrylamido-2-methylpropanesulfonic acid); PCL, poly(ε-caprolactone); PEO, poly(ethylene oxide); PEUU, poly(ester-urethane)urea; PGA, poly(glycolic acid); PHBV, poly (3-hydroxybutyrate-co-3-hydroxyvalerate); PLA, poly(lactic acid); PLAGA, poly(lactic acid-co-glycolic acid); PLGA, poly(lactide-*co*-glycolide); PLLA, poly(L-lactic acid); PLLCL, poly(L-lactic acid)-co-poly(3-caprolactone); PPV, poly(p-phenylenevinylene); PS, polystyrene; PU, polyurethane; PVA, polyvinyl alcohol; PVP, polyvinyl pyrrolidone; RGD, Arg-Gly-Asp; SF, silk fibroin; TCP, tricalcium phosphate.

* Corresponding author at: College of Physics, Qingdao University, Qingdao 266071, China.
** Corresponding author.
E-mail addresses: yunze.long@163.com (Y.Z. Long), xingyujiang@nanoctr.cn (X.Y. Jiang).

0079-6700/$ – see front matter © 2013 Elsevier Ltd. All rights reserved.
http://dx.doi.org/10.1016/j.progpolymsci.2013.06.002

2.1.3. Fiber solidification and deposition ... 867
2.2. Processing parameters ... 867
3. Electrospun 3D fibrous macrostructures ... 868
3.1. Multilayering electrospinning ... 868
3.2. Post-processing after electrospinning ... 870
3.3. Liquid-assisted collection ... 871
3.4. Template-assisted collection ... 872
3.4.1. Using a mechanical collector ... 872
3.4.2. Using a fibrous matrix ... 873
3.5. Adding porogen ... 873
4. Self-assembled 3D electrospun fibrous structures ... 874
4.1. Honeycomb structure ... 875
4.2. Nanofiber yarns ... 875
4.3. Fibrous stacks ... 876
4.4. Other methods ... 877
5. Applications ... 878
5.1. Tissue engineering ... 879
5.1.1. Guidance of cell outgrowth and nerve regeneration ... 879
5.1.2. Vascular grafts ... 879
5.1.3. Bone regeneration ... 881
5.1.4. Skin tissue engineering ... 882
5.2. Energy harvest and storage materials ... 883
5.3. Filtration ... 883
6. Challenges in electrospinning ... 885
7. Summary and outlook ... 885
Acknowledgments ... 886
References ... 886

1. Introduction

Nowadays, materials based on one-dimensional (1D) nanostructures (e.g., nanofibers, nanotubes, nanorods, nanowires, nanobelts) have created a subject of substantial interest due to their unique properties, such as size effects, surface effects, superparamagnetism, and resulting intriguing applications in many fields, including sensors, solar cells, nanoresonators, and so on [1–4]. Among these 1D nanostructures, nanofibers, which have large length/diameter ratio and diameters, from tens to hundreds of nanometers, as well as an enormous surface area per unit mass, have been widely applied in practice due to their ease in production process compared with other nanostructured materials. Up to now, a range of techniques such as drawing, template synthesis, phase separation, self-assembly, and electrospinning, etc. have been adopted to prepare nanofibers based on polymers, metals, ceramics and glass, etc. [5,6], as well as their further assemblies into two dimensional (2D) and three-dimensional (3D) nanostructures for practical applications.

Compared with their 2D counterparts, 3D nanostructures with a significant thickness are increasingly being investigated for applications requiring a third dimension/direction, such as solar cells and tissue engineering. For example, by virtue of enhanced optical absorption and photo-carrier collection efficiency, dye-sensitized solar cells (DSSC) based on a 3D ZnO nanowire arrays have a full-sun efficiency 120% higher than the highest value reported for dye-sensitized solar cells based on a 2D ZnO structure [7]. Besides energy harvest and storage, another important application of 3D fibrous nanostructures is tissue engineering, an emerging interdisciplinary and multidisciplinary research field involving the use of living cells to develop biological substitutes for implant into the body and/or to foster remodeling of tissues in some active manner [8–10]. From the basic principle of tissue engineering (as shown in Fig. 1), one of the core technologies intrinsic to this effort is artificially engineered scaffold construct technology, which focuses on designing, manufacturing and charactering 3D scaffolds for cell seeding and in vitro or in vivo culturing. 3D scaffolds can provide a better link between single cells and organs than traditional 2D cultures because the 3D scaffold offers another direction for cell–cell interactions, cell migration and cell morphogenesis, which is important in regulating the cell cycle and tissue functions [11]. Various approaches for the fabrication of 3D nanostructures including etching, template-assisted synthesis, solvent casting, particulate leaching, gas foaming, contact printing, wet-chemical approach, electrospinning, lithographic techniques, etc., have been reported in the past decades [7,12–19]. However, a few 3D nanostructures have low porosities, small pore size (on nanoscale or less than 1 μm), and poor pore distribution, resulting in the pseudo 3D structures, which may hinder their further applications in some specific areas. For example, the comparative size of a rounded cell is generally in the range of 5–20 μm, which means that the aforementioned pore size is too small to accommodate normal cells and will obstruct cellular migration [20]. Furthermore, 3D microenvironments and interconnectivity are also important for cellular motility and reorganization, not only to provide the template for cells to adhere and grow, but also the interconnectivity facilitates transport of nutrients and metabolites in and out of the engineered tissue. 3D fibrous materials with microstructures and nanotextures

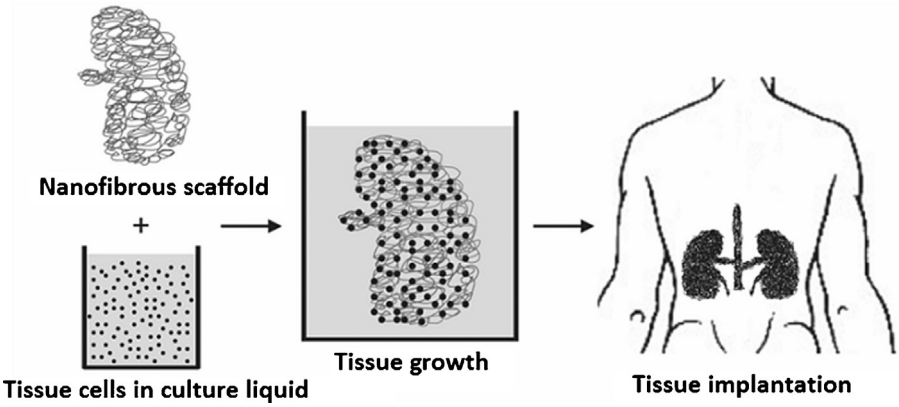

Fig. 1. Illustration of tissue engineering, which includes several core technologies: scaffold construction, cell seeding and culture, and technologies for in vivo integration [10], Copyright 2008. Reproduced with permission from Springer-Verlag.

address these limitations through their high porosities (up to 95%), isotropic structures, and homogeneous fiber size (1–1000 μm) [11]. Simultaneously, these structures have thicknesses ranging from a few times than the diameter of a rounded cell to a millimeter-scale (3D fibrous macro-structures) that provides a spatially distribututed interconnected pore structure that is essential for tissue ingrowth, vascularization, and diffusion of nutrients [20].

Significant efforts have been invested in developing different methods for the assembly of 3D fibrous structures such as microembossing [12], fiber felts [19,23], fiber bonding [21,23], and needle punch [22], 3D printing [22], electrospinning [24], etc. Their advantages and disadvantages are summarized in Table 1. Among these techniques, electrospinning is regarded as a simple and versatile top-down approach for fabricating uniform ultrafine fibers in a continuous process and at long length scales. Since electrospinning has some advantages, such as the facile control of porosity, fiber size, and morphology, much effort has been taken to fabricate micro/nanofibers with desired morphologies, such as aligned fibrous array, fibrous patterns. [3,24–29]. Nevertheless, scalable and controllable assembly of nanofibers for 3D fibrous structures still presents a major challenge because most of the electrospun nanofibers are limited to the conventional 2D membranes. In general, there are four main strategies for the fabrication of 3D electrospun fibrous macro-structures: (a) increasing spinning time; (b) assembly by post-processing of 2D electrospun fibrous structures (e.g., folding, layer-by-layer electrospinning, sintering, mechanical expansion); (c) direct assembly by an auxiliary factor (e.g., a 3D template, liquid collector); (d) self-assembly. In this review, we briefly summarize recent advances in the formation of 3D electrospun fibrous macro-structures technologies, including multilayer electrospinning, post-processing of the as-spun fibers, using 3D collectors or liquid collectors, and self-assembly. These 3D electrospun fibrous macro-structures demonstrate many promising potential and practical approaches to some fields such as tissue engineering, energy harvesting, filters, catalyst supports, micro-containers, and so on, due to their relatively large surface area and pore size compared with the 2D mats.

2. Electrospinning background

The principle of electrospinning was first studied by Formhals in the 1930s [30], regaining considerable attention in the 1990s [31]. A typical electrospinning setup is composed of three basic elements: a high voltage DC (or AC) power supply, a capillary (including a solution container and a spinneret) and a grounded metal collector (usually aluminum foil). One electrode of the high voltage power supply is connected with the spinneret containing spinning solution/melt and the other attached to the collector, which is usually grounded, as shown in Fig. 2a. When electrospinning, the precursor solution is extruded from a spinneret to form a small droplet in the presence of an electric field, and then the charged solution jets are extruded from the cone. Generally the fluid extension occurs first in uniform filaments, and then the straight flow lines undergo vigorous whipping and/or splitting motion due to fluid and electrically driven bending instabilities. Finally, the continuous as-spun fibers are deposited, commonly as a 2D nonwoven web on the collector (Fig. 2b). Besides fiber mesh without orientation, as shown in Fig. 2c–i, other fiber morphologies and structures (e.g., parallel and crossed fiber arrays, helical or wavy fibers, twisted fiber yarns, patterned fiber web, and 3D fibrous stacks) also can be obtained via modified electrospinning process or collectors. In the past decades, a variety of micro/nanofibers from a remarkable range of organic and inorganic materials have been electrospun successfully. And their specific physical and chemical properties make them have widely applications in many fields such as optoelectronics, sensors, catalysis, textiles, filters, fiber reinforcement, tissue engineering, drug delivery, and wound healing etc. [32–39]. There are a variety of parameters that influence the morphology and diameter of the electrospun fibers, including the intrinsic properties of the solution (e.g., the type of polymer, the conformation of polymer chain, viscosity/concentration, elasticity, electrical conductivity, and the polarity and surface tension of the solvent), the operational conditions (e.g., the strength of applied electric field, the distance between spinneret and the collector, and the feeding rate for the polymer solution), as well as the humidity and temperature of the surroundings.

Table 1
Some fabrication methods for 3D fibrous scaffolds.

Method	Advantages	Disadvantages	References
Fiber bonding	High porosity	Hard to control porosity and lack required mechanical strength for the load-bearing tissues	[21,23]
Fiber felts	Easy process and high porosity	Lack structural stability	[19,23]
Needle punch	High porosity	Hard to control pore size	[11,22]
Microembossing	Controlled pore size	Small porosity	[11,12]
3D printing	Controlled pore size	Small porosity	[11,22]
Electrospinning	Controlling of porosity, fiber size, morphology	Low porosity	[24]

2.1. Electrospinning process

The electrospinning process presents an electrified fluid dynamics related problem. In order to control the morphology, structure, and mass production of the electrospun nanofibers, it is necessary to understand quantitatively how the electrospinning process transforms the fluid solution through a millimeter diameter capillary tube into solid micro/nanofibers which are four to five orders of magnitude smaller in diameter. Recent theoretical and experimental studies have demonstrated that the electrospinning process generally consists of three stages: (1) jet initiation and elongation of the charged jet along a straight line; (2) growth of electrical bending instability (also known as whipping instability) and further elongation of the jet, which may or may not be accompanied with the jet branching and/or splitting; (3) solidification of the jet into micro/nanofibers and deposition on collector.

2.1.1. Jet initiation and straight elongation

The electric force has been identified as the driving force for initiating an electrospinning process. In needle electrospinning, under the influence of electric force, the charged solution droplet at the needle tip reduces its size so that the force balance is maintained. With an increase in the applied voltage, the shape of the solution droplet evolves from the hemisphere to a cone shape (Taylor cone) with a high electric force concentrated at the tip of the Taylor cone [40]. When the electric field reaches a critical voltage V_c, the droplet at the cone tip overcomes its surface tension to eject into the electric field, and a solution jet is thus generated. According to Taylor's calculation, the critical voltage V_c (expressed in kilovolts) for electrospinning is given by [41]

$$V_c^2 = 4\frac{H^2}{h^2}\left(\ln\left(\frac{2h}{R}\right) - 1.5\right)(1.3\pi R\gamma)(0.09) \quad (1)$$

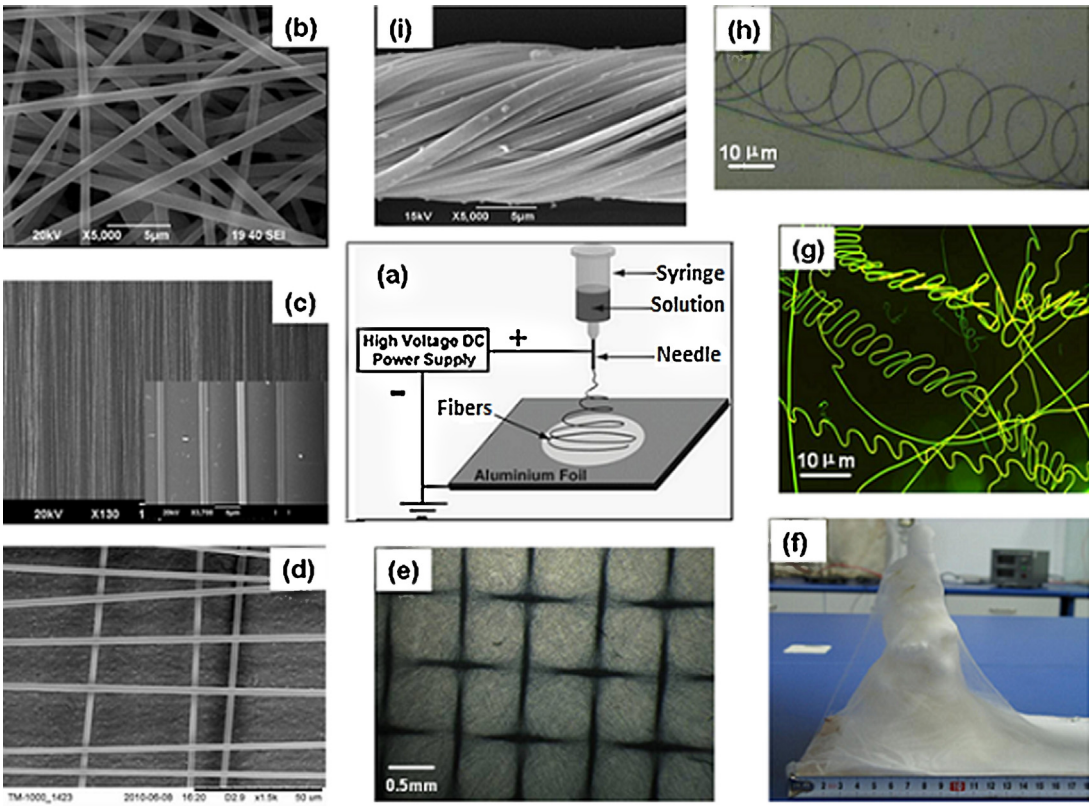

Fig. 2. (a) Schematic diagram of electrospinning method, (b) electrospun polymer nanofiber mesh without orientation, (c) parallel and (d) crossed fiber array, (e) patterned fiber web, (f) 3D fibrous stack, (g) wavy and (h) helical fibers, and (i) twisted fiber yarns.

where H is the distance from the needle tip to the collecting screen, h is the length of the liquid column, R is the needle outer radius, and γ is the surface tension of the solution (units: H, h and R in cm, γ in dyn per cm); the factor 0.09 is inserted to express the voltage in kilovolts.

In the case of needleless electrospinning or free-surface electrospinning, Lukas et al. explained the self-organization of jets developing on a free liquid surface in the spinning process [42]. The critical electric field intensity for electrospinning nanofibers was proposed as:

$$E_c = \sqrt[4]{4\gamma\rho g/\varepsilon^2} \tag{2}$$

where ρ is the liquid mass density, g is the gravity acceleration, γ is the surface tension of the solution, ε is the permittivity. In both the models, electric force plays a crucial role in the jet initiation.

Before the growth of electrical bending instability, the straight, tapered segment of the jet leaving the tip is accelerated as the Coulomb forces, acting on the charges carried with the leading segments, pull the jet toward the collector. The velocity of the electrospinning jet has been estimated using a moving substrate and high-speed camera to be about 1–15 m s^{-1} [43]. The critical length of the straight jet (L) in electrospinning also can be estimated by the following equation proposed by He et al. [44]:

$$L = \frac{4kQ^3}{\pi\rho^2 I^2}(R_0^{-2} - r_0^{-2}) \tag{3}$$

where $R_0 = (2\sigma Q/\pi k\rho E)^{1/3}$, Q is the flow rate, σ is the surface charge, k is the dimensionless conductivity, E is the applied electric field, I is the current passing through the jet, ρ is the liquid density and r_0 is the initial radius of the jet. It is found that the theoretic prediction was in well agreement with the experimental observations for poly(hydroxybutyrate-*co*-valerate) (PHBV) and cellulose solutions [44].

2.1.2. Growth of bending instability and further elongation

As the diameter of the jet, in the straight segment, decreases monotonically with distance from the tip, the jet becomes very long and thin, and the characteristic time required for excess charge to redistribute itself along the full length of the jet becomes longer. The location of excess charge, within or on the fluid, then tends to change with the elongation, bending and otherwise deforming the jet. That means the long jet becomes unstable due to the growth of various instabilities. In fact, recent studies have demonstrated that the key role in reducing the jet diameter from a micrometer to a nanometer is played by a non axisymmetric or electrically driven bending instability, which causes bending and stretching of the jet at very high frequencies. As shown in Fig. 3, Reneker and coworkers [45–47] described the path of the jet as a straight segment followed by a series of successively smaller electrically driven bending coils, with each bending coil having turns of increasing radius. The elongation of each segment by the electrical forces caused by the charge carried with the jet continues.

Reneker and coworkers [45,46], Shin et al. [48,49] and Hohman et al. [50,51] investigated mathematical expositions and asymptotic analyses to model the instabilities.

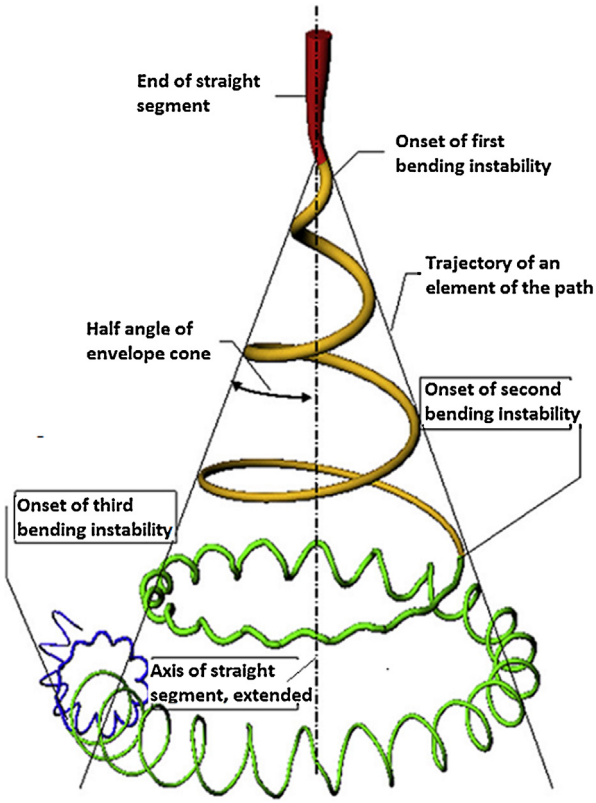

Fig. 3. Diagram that shows the prototypical instantaneous position of the path of an electrospinning jet that contains three successive electrical bending instabilities [47], Copyright 2008. Reproduced with permission from Elsevier Ltd.

They found that the possibility for three types of instabilities exists. The first is the classical Rayleigh instability, which is an axisymmetric instability dominated by surface tension and suppressed at high electric fields when the applied electric field E_0 and the surface charge density σ exceed a threshold given by:

$$(\varepsilon - \varepsilon')E_0^2 + 4\pi^2\sigma^2/\varepsilon' = 2\pi\gamma/h \tag{4}$$

where γ is the surface tension, h is the radius of the jet, ε and ε' are the dielectric constant inside and outside the jet separately, and $\varepsilon/\varepsilon' \gg 1$. The second is again an axisymmetric instability, which is usually referred to as the second axisymmetric instability, and occurs at higher electric field than the Rayleigh instability. The third is a non axisymmetric instability (also known as bending or whipping instability), which describes long wave perturbations of a liquid column driven by the lateral electric force and the aerodynamic interaction at high electric field. The latter two are due to fluctuations in the dipolar component of the charge distribution. They are electrically driven and essentially independent of the surface tension of the liquid. It is noted that the electric field strength will be proportional to the instability level. Namely, the Rayleigh instability occurs when the electric field is the lowest, whereas the bending instability corresponds to the highest electric field [48]. In particular, Fridrikh et al. [52] proposed a model applicable to a charged liquid in an electric field

with bending instability that predicted the diameter of a terminal jet:

$$h_t = \left(\gamma\varepsilon' \frac{Q^2}{I^2} \frac{2}{\pi(2\ln\chi - 3)}\right)^{1/3} \quad (5)$$

where h_t is the terminal jet diameter, Q is flow rate, I is electric current, γ is surface tension of the liquid, ε' is dielectric constant of the medium surrounding the jet, and $\chi \sim R/h$ is the dimensionless wavelength of the bending instability (R is the radius of the bending perturbation and h is the jet radius). They also found that theoretical predictions were in agreement with experimental data obtained from electrospinning PCL solutions.

It should be noted that in addition to the electrical bending instability, other characteristic instabilities such as branching and formation of physical beads have also been observed. For example, as the jet fluid driven by the electric forces is unstable during its trajectory toward the collector, branching and/or splitting from the primary jet should be possible. If the excess charge density on the surface of the jet is high, undulations are predicted to form on the surface of a cylindrical jet. These undulations grow large enough to become unstable, and initiated branches which grow outward from the primary jet. A theoretical model for the evolution of an electrically charged fluid jet into a branched jet was developed by Yarin et al. [53]. The formation of branches is observed more frequently in more concentrated and more viscous solutions, and at electric fields higher than the minimum field required for producing a single jet. In addition, when the excess electrical charge carried by the jet is reduced, the capillary instability, which causes a cylindrical fluid jet to break up into droplets, may occur and lead to formation of beaded nanofibers [54,55]. It is noted that branches occur when the charge per unit area is large, with beads occurring when the charge per unit area is small.

2.1.3. Fiber solidification and deposition

During the process of jet elongation, the solvent evaporates, leaving behind a charged polymer fiber. Yarin et al. [46] derived a quasi-1D equation to describe the mass decrease and volume variation of the fluid jet due to evaporation and solidification. They calculated that the cross-sectional radius of the dry fiber was 1.3×10^{-3} times of that of the initial fluid jet. The effect of evaporation and associated solidification of the charged jet of poly(ethylene oxide) aqueous solution was further studied by Reneker and coworkers [56] by varying the relative humidity during electrospinning. As the relative humidity increases, the solidification process becomes slower, allowing elongation of the charged jet to continue longer and thereby to form thinner fibers. The solid polymer fibers are then deposited on a grounded collecting screen. During the fiber deposition process, a characteristic instability termed as buckling instability may occur due to the longitudinal compressive force from jet impingement on a solid flat surface. This instability usually results in bending fibrous structures with sinuous folding and overlapping figures-of-eight and circles with frequencies of the order of 10^5 to 10^6 Hz (for comparison, the electrical bending loops are formed at the frequencies of the order of 10^3 Hz). The buckling patterns have been widely observed in fiber depositing on a hard flat surface from both uncharged and electrified jets [57].

In particular, the morphology and structure of the deposited fibers are strongly dependent on the collection method. Besides randomly oriented fiber mat collected by a stationary plate, other collector configurations such as a rotating mandrel, frame, solvent bath, auxiliary electric or magnetic field, etc. have been used to collect well aligned fiber array, patterned fiber mat, fiber yarn or rope, tubular construct, and other 3D fibrous scaffolds, etc. This ease of use and adaptability extends the possible applications of electrospun nanofibers.

2.2. Processing parameters

Altough electrospinning is relatively easy to use, many parameters can greatly influence the transformation of polymer solutions into nanofibers. These include (a) the solution properties such as viscosity, conductivity, and surface tension, (b) working voltage applied at the spinneret tip, spinning distance between the tip and the collector surface, and polymer flow rate and (c) ambient parameters such as solution temperature, humidity, etc. The effects of electrospinning parameters on fiber morphology have been widely explored for different systems [58–61]. For example, Zheng et al. [61] carried out a series of experiments to study the influence of processing variables (solution concentration, spinning distance, collecting position and humidity) on the formation of near-field electrospun polyvinyl pyrrolidone (PVP) with a working voltage of less than 2.8 kV and a spinning distance of less than 10 mm. They found that no fibers were collected when the PVP concentration was too low (<20 wt%) to attach to the spinning tip or the PVP concentration was too high (>40 wt%) to produce a spinning jet. A mixture of beaded fibers and uniform fibers was obtained when the PVP loading was 25 wt%, and totally uniform fibers were collected as the PVP concentration increased to 30 and 35 wt%. Moreover, the average diameter of the nonwoven fibers electrospun from the 35 wt% solution was 690 nm, much larger than that from the 30 wt% solution (~310 nm) due to higher viscosity. These results indicate that the viscosity (solution concentration) has a significant effect on the fiber formation. At low viscosities, solution surface tension in the dominant influence on fiber morphology and below a certain concentration drops will form instead of fibers. At high concentrations, electrospinning is prohibited by an inability to control and maintain the flow of a polymer solution to the nozzle. In addition, a higher polymer concentration tends to stabilize the jet and results in fewer beads (beaded fibers) and more uniform fibers [55].

In addition to viscosity (solution concentration), the effects of other parameters such as flow rate, distance from nozzle to collector, initial jet/orifice radius, electric potential, relative humidity, etc. on nanofiber diameter have been explored systematically by Thompson et al. [62]

(a) Initial jet/orifice radius: decreasing orifice radius tends to decrease the average fiber diameters (e.g., average

fiber diameters of 250, 150 and 125 nm for orifices of radii 0.59, 0.42 and 0.29 mm, respectively) [63].

(b) Flow rate: increasing flow rate tends to increase fiber diameter [55,64].

(c) Distance from nozzle to collector: average fiber diameters tend to decrease with increase in collector distance [55,64,65]. For example, Nylon-6 fiber diameters decrease from 230 to 140 nm with spinning distance changing from 4 to 18 cm, holding other parameters constant [65].

(d) Polymer concentration: Nylon-6 fiber diameters increase from 80 to 230 nm when increasing initial polymer concentration from 10 to 25% [65].

(e) Applied voltage: in general, a higher applied voltage ejects more fluid in a jet, resulting in a larger fiber diameter [66,67]. However, Katti et al. [63] reported an initial decrease in diameter of poly(lactide-*co*-glycolide) fibers from 900 to 450 nm with an increase in applied voltage from 8 to 10 kV (electric field strength of 0.4–0.5 kV/cm).

(f) Vapor diffusivity: lower evaporating solvent allowing for longer stretching process before jet solidification taking place, and thus for thinner fibers [62].

(g) Relative humidity: as the relative humidity increases, the solidification process becomes slower, allowing elongation of the charged jet to continue longer and thereby to form thinner fibers. For example, as the relative humidity increases from 5.1% to 48.7%, the diameter of the solidified PEO fibers decreases from 253 to 144 nm [56].

(h) Solution conductivity: increasing solution conductivity tends to decrease fiber diameter due to increase in electrical charge carried by the jet and thus tensile force in the presence of an electric field. For example, by adding increasing concentrations of NaCl (ranging from 0.05 to 0.2%, the corresponding solution conductivity increased from 1.53 to 10.5 mS/cm), Zhang et al. [68] were able to decrease the mean fiber diameter from 214 ± 19 to 159 ± 21 nm.

(i) Surface tension: the effect of surface tension is negligibly small for most properly chosen electrospun solutions, where the viscoelastic forces completely dominate the surface tension [62]. However, for higher surface tension solvents like water, low viscosity and low conductivity/charge density systems beaded fibers tend to form.

Table 2 shows a summary of the effects of electrospinning parameters on fiber diameter. It is evident that increasing spinning distance and solution conductivity can decrease fiber diameter, whereas increasing flow rate and polymer concentration (viscosity) can result in larger fiber diameter.

3. Electrospun 3D fibrous macrostructures

Several approaches to electrospinning 3D fibrous macro-structures have been realized. As shown in Fig. 4a, one simple way is sequential electrospinning or multilayering electrospinning. In this way, electrospun fiber membrane with a certain thickness will be obtained, which can reach hundreds of microns and become a 3D fibrous structure, although these methods may take a long time (for example, from 20 min to 20 h) till it grows to a sufficient 3D structure. Another way is post-processing of the electrospun fibers, such as peeling off the thin film from the collector, and then bending/folding or stacking the fiber layers into a 3D fibrous structure like pipe or thick mat (Fig. 4b). In addition, 3D fiber structures can be also successfully obtained through modification of the collector, for example, replacing the conventional 2D flat collector by a 3D collecting template (Fig. 4c). In addition, other methods such as using liquid collection and removing microparticles filled between nanofibers have been reported, although a subsequent treatment to dry the as-prepared 3D structures or handle with the porogen is usually needed. Furthermore, by controlling some parameters during the electrospinning process (e.g., the solution concentration/viscosity, electrostatic field, ambient humidity), a rapid growth (or self-assembly) of 3D fibrous macro-structures has been achieved without any additional assistance (e.g., fibrous yarns or spongiform fiber stacks), as shown in Fig. 4d. Various 3D fibrous macro-structures are reviewed in this section, including multi-layer meshes, cotton-like stacks, multiple interconnected tubes, nano-/microfibrous hybrid scaffolds, fibrous yarns, etc., which have been electrospun successfully.

3.1. Multilayering electrospinning

As emphasized in the preceding, electrospinning is suitable for fabricating porous fibers, especially the 2D structures including random oriented mats, as well as aligned fibrous arrays. It is of evidence that mat thickness increases by increasing spinning time during the conventional electrospinning process, leading to a 3D fibrous structure with the thickness from tens to hundreds of microns. Furthermore, a 3D macro-structure can be also realized by coating a layer of nanofibers on another electrospun fiber layer. Namely, 3D multilayered fibrous membranes of different materials can be fabricated by a sequential electrospinning [69] or co-electrospinning (Fig. 5a) [70], and sometimes an auxiliary electric field is even used to converge the collected fibers into a confined space to produce 3D fibrous structures [71]. For example, by exchanging and alternately electrospinning two polymer solutions under different conditions, Pham et al. [71] prepared layer-on-layer stacks including alternating layers of PCL microfibers and PCL nanofibers. This proposed 3D structure combined the beneficial properties of nanofibers with that of microfibers. Fig. 5b shows the cross-sectional images of the scaffolds consisting three nano/microfiber layers with different thickness (spinning time was 30 s, 90 s and 5 min, respectively). The total thickness of the multilayers was greater than 1 mm. The average pore size of microfiber scaffolds was dependent on its fiber diameter and ranged from 10 to 45 μm, while the porosities were nearly constant, between 84% and 89%. In addition, by varying the solutions and processing parameters, 3D scaffold with three different layers (dense layer, cellular layer, and porous layer) from cellulose acetate have also been electrospun [72]. As shown in Fig. 5c, these sandwiched configurations, which mimic the natural architecture of extracellular matrix, may reduce

Table 2
Effects of processing parameters on electrospun fiber diameter.

Parameter	Effect on fiber diameter	Explanation	References
Orifice radius/initial jet	Decreasing orifice radius tends to decrease the average fiber diameters	The size of initial jet decreases	[63]
Flow rate	Decreasing flow rate tends to decrease fiber diameter	A lower flow rate ejects less fluid in a jet	[55,64]
Distance from nozzle to collector	Average fiber diameters tend to decrease with increase in spinning distance	The jet elongation time increases	[55,64,65]
Polymer concentration/viscosity	Average fiber diameters increase when increasing polymer concentration	The jet elongation becomes more difficult and slower	[61,65]
Applied voltage	Generally, increasing applied voltage results in a larger fiber diameter. However, an initial decrease in diameter with increasing applied voltage was also reported.	A higher applied voltage ejects more fluid in a jet	[63,66,67]
Vapor diffusivity	Lower evaporating solvent tends to decrease fiber diameter	Jet stretching process becomes longer before jet solidification taking place	[62]
Relative humidity	Increasing relative humidity tends to decrease fiber diameter	The jet solidification process becomes slower, allowing elongation of the jet to continue longer	[56]
Solution conductivity	Increasing solution conductivity tends to decrease fiber diameter	The electrical charge carried by the jet increases and thus increasing the electric force	[68]
Surface tension	The effect of surface tension on fiber diameter is negligibly small	The viscoelastic forces completely dominate the surface tension	[62]

cell spreading and enhance the expression of differentiated cell function. One advantage of this multilayer electrospinning is that the fiber diameter, composition, and porosity of each electrospun fiber layer and the total number of layers can be controlled and adjustable, which is critical for cell attachment, proliferation, migration, and/or differentiation on a scaffold.

In addition, a modified electrospinning setup is favorable for the fabrication of this multilayer 3D macro-structure. As an example, Erisken et al. [73]

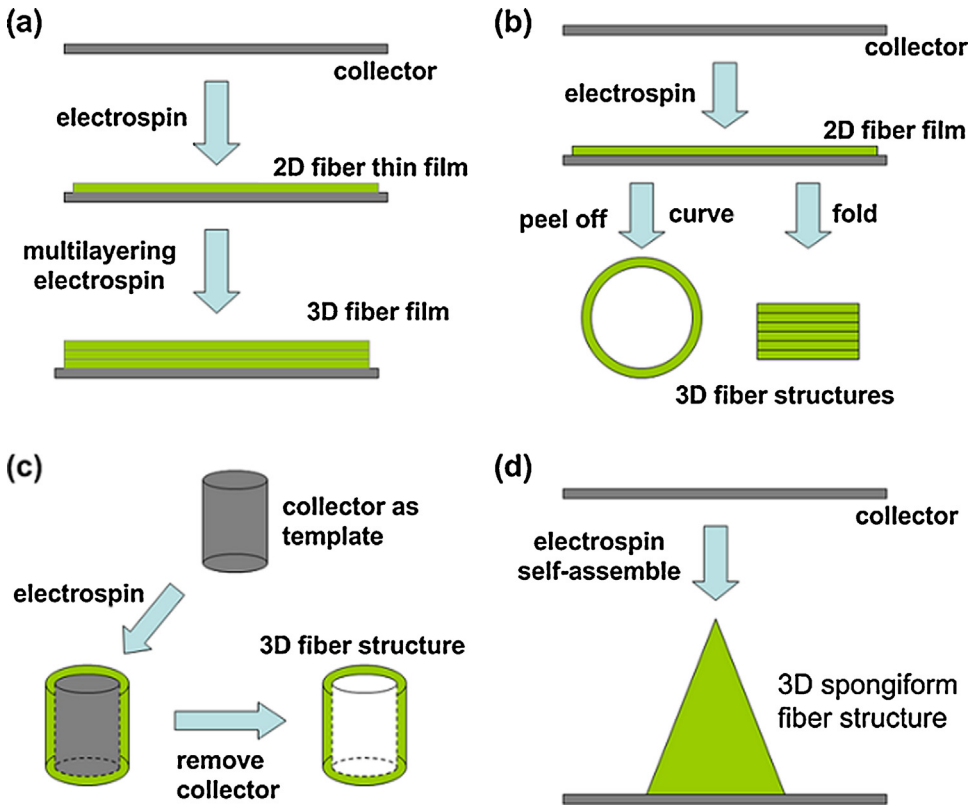

Fig. 4. Schematic illustration of several approaches to fabricate 3D nanofibrous structures via electrospinning: (a) multilayer electrospinning; (b) folding or stacking 2D fiber films; (c) using a 3D collecting template; (d) self-assembly.

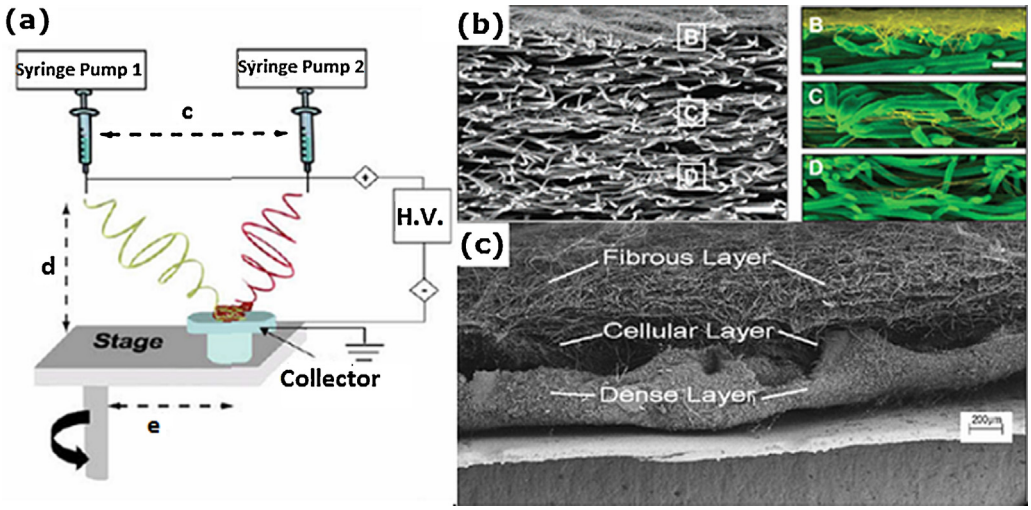

Fig. 5. (a) Schematic representation of the modified electrospinning setup with two parallel syringes and actuated collector target for fabricating multi-layer fibrous meshes [70], Copyright 2010. Reproduced with permission from Elsevier Ltd; (b) 3D nanofibrous structures fabricated by multilayer electrospinning: (A) Cross-section illustrating (from top to bottom) a nano-micro-nano-micro-nano-microfiber layered scaffold. The white boxes correspond to the nanofiber layers and their respective magnified images shown to the right. (B) Magnification of the nanolayer electrospun for 5 min. (C) Magnification of the nanolayer electrospun for 90 s. (D) Magnification of the nanolayer electrospun for 30 s. The scale bar shown for (A) is 100 μm, and for (B–D) it is 25 μm. Microfibers are false colored green while nanofibers are false colored yellow to enhance contrast [71], Copyright 2006. Reproduced with permission from the American Chemical Society; (c) SEM image of the multilayer structured scaffold from cellulose acetate [72], Copyright 2006. Reproduced with permission from Elsevier Ltd.

reported functionally graded electrospun PCL and β-tricalcium phosphate (β-TCP) nanocomposites with a thickness of 0.4 mm using a hybrid twin-screw extrusion/electrospinning process. The ability to incorporate the β-TCP nanoparticles into PCL nanofibers in a controlled manner enabled the better mimicking of the compositional and structural characteristics of the bone tissue particularly at the bone-cartilage interface. Moreover, by virtue of a modified electrospinning setup with two parallel syringes and an actuated collector (co-electrospinning), 3D scaffolds of layered composites with mixed nano- and microscale PCL fibers have been fabricated, allowing different cell types to coexist, with scalability and modularity from an industrial perspective [70].

3.2. Post-processing after electrospinning

With a subsequent post-process after electrospinning such as folding/rolling up, the aforementioned 3D multilayer fibrous structures, even the as-spun 2D layer-on-layer mats, can turn into a desired morphology for further application. For example, 3D macro-structures based on double-layered nano/microfibrous chitosan were prepared by a three-step process: First, chitosan microfibers were fabricated to form sheets with proper pores in advance; and then, nanofibrous chitosan was electrospun to the upper side of microfibers sheet on collector; finally, the double-layered sheets were rolled-up, thus forming the 3D structures [75]. The proposed structures as scaffolds had dual porous architecture containing nanofibrous walls and microsized pores formed by microfibrous sheet. Subsequently in vitro chondrocyte culture in this scaffolds suggested that this material provided a great microenvironment for chondrocytes to proliferate and produce glycosaminoglycan (GAG) very well. Moreover, Wang and cooperators [76,77] have electrospun chitosan nano/microfiber mesh tubes with the aid of a rotating drum (steel use stainless bar). In this case, by controlling the spinning parameters, the chitosan films consisting of nonwoven or oriented fibers deposited and reeled on the bar as the drum rotates. And after removing the rotating bar, chitosan mesh tubes were obtained with an inner diameter of 2.0 mm and an outer diameter of 2.1 mm for the nonwoven, and an inner diameter of 1.2 mm and an outer diameter of 2.0 mm for the oriented (Fig. 6a), respectively. Furthermore, by folding the aligned electrospun nanofibrous meshes several times, a 3D unwoven macroporous nanofibrous scaffold was manufactured. For this structure, the as-spun aligned nanofibrous yarns were compressed into a disk with 3 mm thickness [78]. However, 3D structures generated by this method usually cannot put into use as scaffolds directly because they often have a large space or distance between adjacent fibrous surfaces, and in this case, cells only attach and stretch on the 2D surface, rather than forming bridge between surfaces due to the large distance [11].

Moreover, 3D electrospun poly(L-lactic acid) (PLLA) microfibrous scaffolds with 5 mm in thickness were fabricated by using a subsequent mechanical expansion process (Fig. 6b) [74]. Compared with the electrospun 2D nanofibrous membranes, the 3D scaffolds demonstrated a high level of osteoblast proliferation and could be a favorable substrate for cell infiltration and bone formation.

Sintering after electrospinning is another way to fabricate 3D macro-structures. For example, 3D electrospun scaffolds of pure PLGA and composites of PLGA/hydroxyapatite (HAp) were fabricated [79,80] by a two-step process: About 40 layers of electrospun meshes

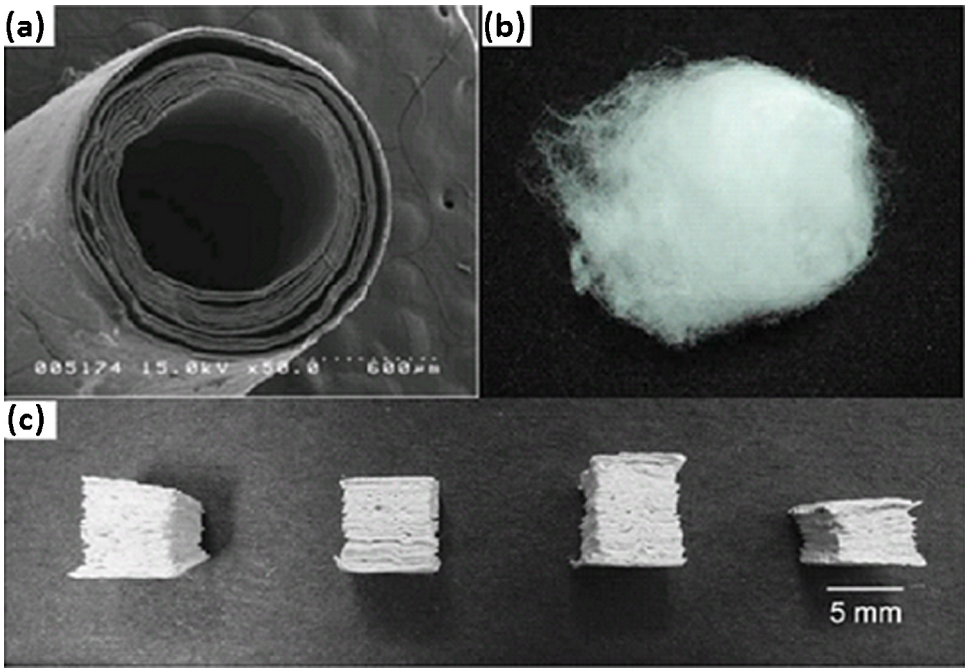

Fig. 6. 3D nanofibrous structures obtained by post-processing after electrospinning: (a) Oriented chitosan mesh tube [77], Copyright 2009. Reproduced with permission from Wiley-VCH Verlag GmbH & Co., KGaA; (b) 3D microfibrous scaffolds after mechanical expansion [74], Copyright 2010. Reproduced with permission from Wiley-VCH Verlag GmbH & Co, KGaA; (c) Picture of 3D composite scaffolds with concentrations of 0, 5, 10, and 20 wt% (from left to right) and processed for 10 s [80], Copyright 2011. Reproduced with permission from Wiley-VCH Verlag GmbH & Co, KGaA.

were stacked, and then sintered using pressurized gas (0.35 kPa). Fig. 6c shows a picture of 3D composite scaffolds with hydroxyapatite concentrations of 0, 5, 10, and 20 wt% (from left to right) and post-processed for 10 s. However, the fibers melted after calcinations leading to the solidification of the layers. In addition, the as-spun 3D structures could be tailored into different patterns by the use of a phase modulated femtosecond laser pulse [81,82]. This technique may provide a useful platform for the fabrication of a variety of functional microstructures by allowing researchers to selectively tailor the topography of porous electrospun mats.

Although the methods described in the preceding permit the fabrication of 3D fibrous macro-structures, they are very slow and inefficient, and not appropriate for production on large scale. Therefore, faster or higher efficient methods are required.

3.3. Liquid-assisted collection

It is known that aligned electrospun micro/nano fibrous arrays can be collected with the help of a water reservoir collector [83] or a water vortex [84]. And this technique is also helpful for fabricating 3D fibrous macro-structures. For example, hierarchically organized 3D nanofibrous meshes of PCL were fabricated with the use of a water vortex [85]. Herein, electrospun fibers are first deposited on the deionized water surface in a receptacle. Simultaneously, a vortex was created as water drained out from an outlet at the base of the receptacle to collect 3D meshes in a reservoir below the receptacle. After collection, the 3D PCL meshes were placed in a mold and were either freeze-dried or dried under room condition. It was found that the collected 3D meshes dried in room condition were dense and compact without any apparent pores on the surface, while the freeze-dried 3D meshes exhibited visible pores on the surface (Fig. 7b), which may be due to the solid/liquid interface energy lower than that of a solid/vapor interface [85].

Other liquids, such as tertiary-butyl alcohol, methanol, and ethanol can be adopted to fabricate 3D fibrous macro-structures because of their lower surface tension than that of pure water. In this process, electrospun fibers deposited into the liquid bath sink. Subsequently, the following electrospun fibers accumulate a relatively fluffy stacks. After a subsequent freezing process at a low temperature (e.g., −70 °C), after the methanol was substituted by distilled water, a foamed 3D structure was prepared, the pore size of the as-prepared 3D structure is much lager than that of 2D nanofibrous mats, and may be considered as excellent scaffolds for 3D cell culture and tissue regeneration. 3D fibrous macro-structures from pure polymer (e.g., silk fibroin, PCL, PLGA, poly(glycolic acid) (PGA)) [86–89] and organic-inorganic composites (e.g., PLLA/vaterite hybrid-composite) [90] have been electrospun successfully in this way. For example, Hong et al. [87] have fabricated size-controlled 3D PCL micro/nanofiber structures by electrospinning the fibers into an ethyl alcohol (EtOH)-containing bath (Fig. 7a). By adjusting the flow rate of EtOH and other electrospinning parameters, the width and height of the 3D fibrous structures were well controlled at the micro/nano scale. In addition, Yokoyama et al. [89] have obtained spongiform nanofiber 3D fabric of poly(glycolic acid) (PGA) by combining electrospinning with wet spinning. Comparing with usual PGA nanofiber

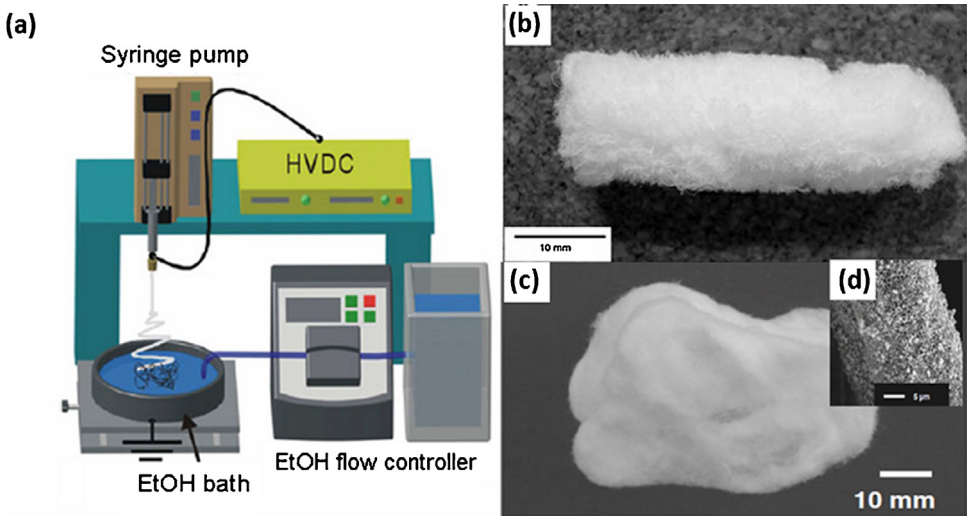

Fig. 7. (a) Schematic of the electrospinning process modified with an EtOH target bath in which the flow of EtOH was controlled with a flow meter [87], Copyright 2011. Reproduced with permission from Springer-Verlag; (b) PCL 3D mesh pre-frozen at −86 °C and freeze-dried in a cylinder with visible pores [85], Copyright 2008. Reproduced with permission from Bentham Science Publishers; (c) entire view of resulting materials of siloxane-doped PLLA/vaterite hybrid-composites; (d) SEM image of the PLLA/vaterite hybrid-composites after alternate soaking treatment using Na_2HPO_4 [90], Copyright 2012. Reproduced with permission from Springer-Verlag.

nonwoven mats prepared by conventional electrospinning method, spongiform PGA nanofiber fabric had a low apparent density and high porosity, indicating its potential application in the structure control of the nanofiber fabric. Recently, Kasuga et al. [90] presented an electrospun 3D siloxane-doped PLLA/vaterite hybrid-composite with a cotton-like morphology. As shown in Fig. 7c, this cotton-like material had a thickness of 40–50 mm. More importantly, the surface of the fiber skeleton could be treated by an alternate soaking method to precipitate calcium phosphates such as hydroxyapatite (Fig. 7d), which was helpful for bone regeneration because it could improve the adhesion of cells at the initial stage after implanting the cotton-like PLLA/vaterite hybrid composites in the body.

The drawback of liquid collection is that an additional molding and freezing process after electrospinning are usually required.

3.4. Template-assisted collection

3D fibrous macro-structures fabricated by template assistance are common nowadays due to the easy controllability. The templates could be shape-desired mechanical collectors (e.g., a rotating collector or a static collector) or some other fibrous structures (e.g., microfibers) acting as matrix templates. In this section, we summarize some significant achievements.

3.4.1. Using a mechanical collector

To our knowledge, the collection of 3D macro-fibrous structures using a mechanical collector was first introduced by Zhang et al. [91], using 3D collecting templates based on manipulation of electric field and electric forces to fabricate micro- and macro single tubes with multiple micropatterns, multiple interconnected tubes and tubes with same or different sizes, shapes, structures and patterns. Fig. 8a and b show the process for fabrication of tubes with a multiple interconnected tubular structure and the as-prepared crossing fibrous tube. It is found that the distance between the individual 3D collectors is a key parameter for the batch fabrication of tubes with different sizes, shapes, wall structures, and patterns. Namely, excessively small distance may cause fiber suspension between collectors. However, manipulation of the electric field is the basic principle of this technique. In their further work [92], 3D tubular fabrics of hydroxyapatite (HAp) nanorods/PVP composite have been fabricated by changing the collectors during electrospinning. After a subsequent thermal treatment at 600 °C for 6 h, the as prepared 3D fabric was used as the substrate for mesenchymal stem cells culture, and the results showed that the scaffold was biocompatible and that cells attach well to it. Additionally, others have investigated the fabrication of 3D fibrous structures by a variety of methods, such as directly rotary jet-spinning [93], a rotating collector [94–98], and so forth. For example, using a rotary jet-spinning combined the hydrostatic pressure with centrifugal pressure, 3D nanofiber structures from poly(lactic acid) (PLA) (Fig. 8c) have been fabricated under a proper rotation speed (e.g., 12,000 rpm) [93], and the contained aligned nanofibers with diameters ranging from 50 to 3500 nm (Fig. 8d), are similar to that of the conventional 2D mats. The rotating collector assists the collection of 3D nanofibrous tubular scaffolds. These as-spun tubular scaffolds with inner diameters of several micrometers, thickness of about 0.5 mm, and the length about several centimeters, even with a patterned morphology [96], are composed of nonwoven or aligned micro/nanofibers. And they usually are adopted for the neural regeneration [98], cell culture [94], vascular graft [95–97], etc. Zhou et al. [95] have analyzed the influence of electrospinning parameters on the morphology and diameter distribution of regenerated silk fibroin in the tubular scaffold. They found that

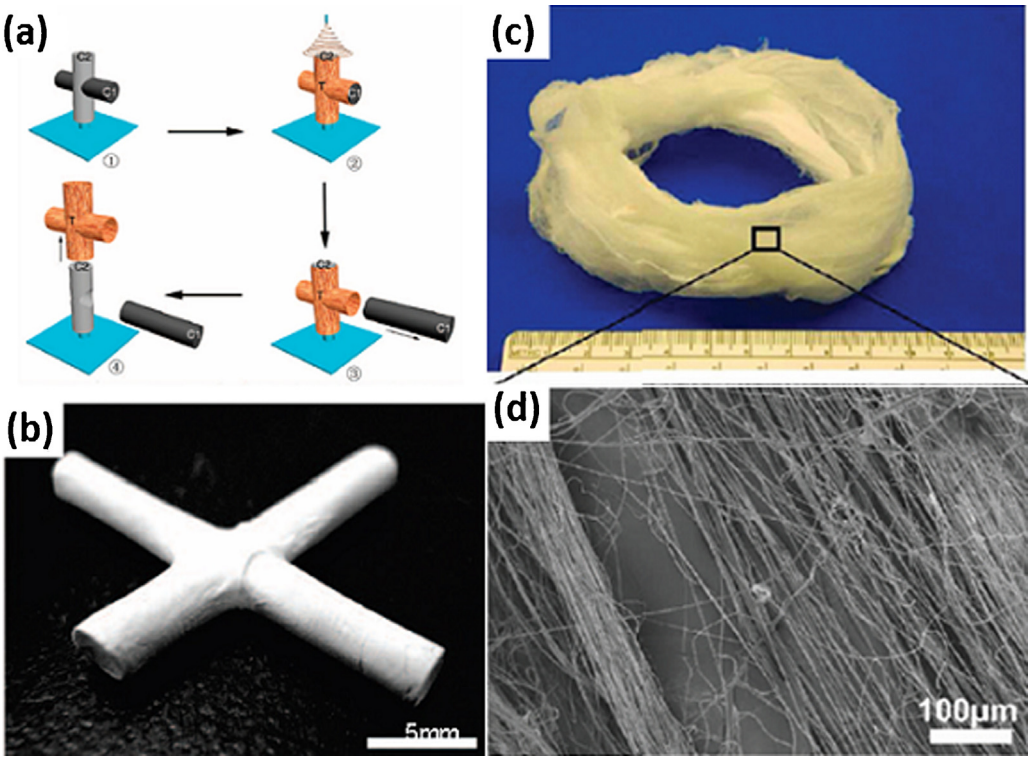

Fig. 8. (a) Schematic illustration of process for fabrication of tubes with multiple interconnected tubular structures; (b) a crossing tube [91], Copyright 2008. Reproduced with permission from the American Chemical Society; (c) photographic image of 3D nanofiber structures produced by rotary jet-spinning, 8 wt% PLA in $CHCl_3$ at 12,000 rpm rotation speed; (d) SEM image of fibers in panel (c) [93], Copyright 2010. Reproduced with permission from the American Chemical Society.

the spinning voltage and concentration had some effect on the average fiber diameter, while collection distance and flow rate were found to significantly affect the fiber uniformity. Moreover, using a rotating drum covered by Al foil, Schneider et al. [99] have fabricated PLGA/tricalcium phosphate (TCP) composite scaffolds with a cotton-like appearance via low-temperature electrospinning. The drum was loaded with dry ice that caused rapid deposition of ice crystals at the cold external cylinder surface on which the fibers were collected.

3.4.2. Using a fibrous matrix

Apart from mechanical collectors, it is also possible to obtain 3D fibrous macro-structures using a matrix. Here the matrix usually is microfibers which are fabricated by other methods in advance or at the same time with electrospinning. Namely, in this case, 3D structures are usually fabricated via a hybrid technique that combines traditional electrospinning with other methods such as prototyping [100,101], polymer/fiber deposition [102,103], melt electrospinning [104], and so on. For example, by combining direct polymer melt deposition (DPMD) with electrospinning, highly functionalized 3D scaffolds were fabricated [103]. As shown in Fig. 9a, a microfiber layer was built by using the DPMD process firstly. Then the microfiber layer was covered by a polymeric nanofiber matrix. 3D hybrid structures were fabricated by electrospinning PCL/collagen biocomposite nanofiber matrices into the microfibrous structures (Fig. 9b). The as-prepared 3D woodpile structure of the hybrid scaffold was composed of PCL microfibrous layers with lengths of 10 ± 0.5 mm and diameters of 350 ± 10 μm and PCL/collagen fibers with diameters of 325 ± 128 nm (Fig. 9c). Cell culture studies revealed that nano-topographical features on the surface of the hybrid scaffolds, chemical composition of the biocomposite and an enlarged inner surface of the structure resulted in a significant improvement in terms of cell adhesion and proliferation [103,105]. In addition, 3D nano-/microfibrous PLGA scaffolds with the thickness up to 2–3 cm were fabricated by hybrid electrospinning including a solution electrospinning and melt electrospinning [104] (Fig. 9d), which consisted of a randomly oriented structure of PLGA microfibers (average fiber diameter = 28 μm) and PLGA nanofibers (average fiber diameter = 530 nm) (Fig. 9e). These scaffolds were examined and compared with the PLGA microfiber scaffolds in terms of the attachment, spreading and infiltration of normal human epidermal keratinocytes and fibroblasts. The cell attachment and spreading of both cell types were several times higher in the nano-/microfiber composite scaffolds than in the microfibrous scaffolds without nanofibers.

3.5. Adding porogen

Some materials, such as ice crystals, salt particles, and even some polymers (e.g., poly(ethylene oxide) (PEO))

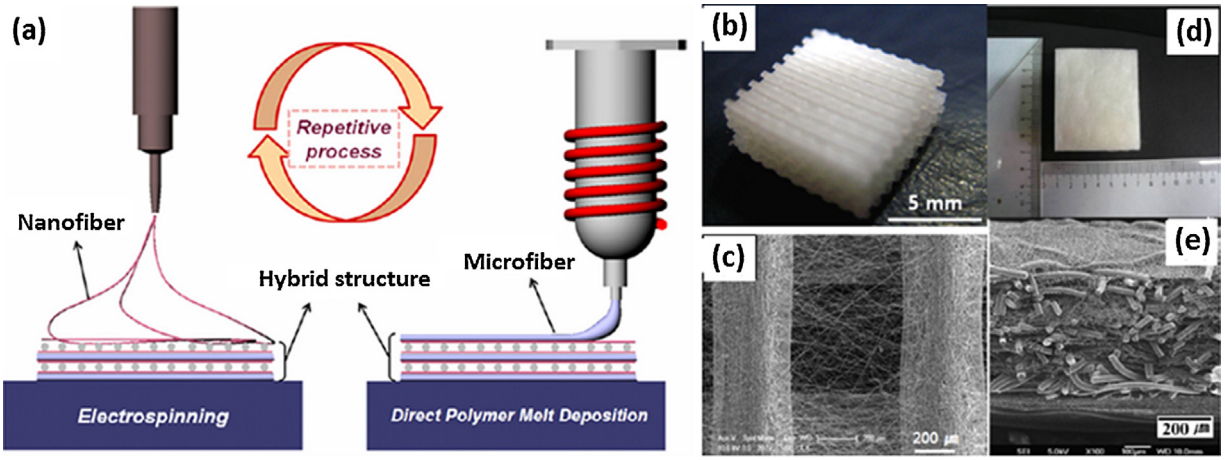

Fig. 9. (a) The developed hybrid process. Hybrid scaffolds containing microfibers and nanofiber matrices could be built via a combined process of continuous DPMD and electrospining; (b) Photograph of the overall 3D woodpile structure with dimensions of 9 mm × 9 mm × 3.5 mm; (c) Magnified image of the hybrid basic unit layer composed of microfibers and the electrospun nanofibers matrix [103], Copyright 2008. Reproduced with permission from Elsevier Ltd; (d) Photographs of PLGA nano-/microfiber composite scaffold; (e) cross-section SEM image of the PLGA nano-/microfiber composite scaffolds [104], Copyright 2010. Reproduced with permission from Elsevier Ltd.

can be adopted for the fabrication of 3D fibrous macrostructures. The materials, acting as porogens, usually are mixed simultaneously with the precursor during electrospinning to enable rapid build-up of the nanofibrous volume, and then washed away or dried after a desired thickness is reached [99,106–110]. For example, by combining particle leaching and electrospinning, Kim et al. [108] successfully fabricated a 3D macroporous and nanofibrous hyaluronic acid scaffold, as shown in Fig. 10a and b. Here the salt particles were simultaneously deposited by an automatic vibration sieving method during the electrospinning procedure with a proportion of either 90% or 80% to the nanofibers. After cross-linking the hyaluronic acid and collagen nanofibers by dipping the scaffold in 1-ethyl-3-(3-dimenthylaminopropyl) carbodiimide hydrochloride (EDC) solution and leaching the salt particles in water, the thickness of the scaffold was reduced by around 50%. It was observed that the scaffolds retained irregular open pore geometry even after cross-linking (Fig. 10c), with macropores defined by nanofibrous walls in which nanopores were also observed. It was confirmed that the macropores (50–100 μm) were largely preserved despite of the extensive swelling of nanofibers. A dually interconnected pore morphology was also observed, characterized by two types of voids: nanopores surrounded by nanofibers and macropores. Moreover, it was concluded from the cell culture study (chondrocyte adhesion and proliferation assessment) that the content of collagen could enhance cell adhesion and growth [105,108].

4. Self-assembled 3D electrospun fibrous structures

Self-assembly, as an important "bottom-up" approach, is intensively studied in chemistry, physics, biology, and materials engineering. It can easily arrange small components into ordered systems (e.g., patterns) or aggregate structures without human intervention, which otherwise will be expensive, slow, and complex. Self-assembling processes are common throughout nature and technology, especially in the field of nanoscale materials. It is one of the few practical strategies for making ensembles of nanostructures, and therefore an essential part of nanotechnology. For example, there are many reports on small components from molecules [111–113] to nanoscale particles [114,115] to be self-assembled into ordered aggregates with desired structures [116].

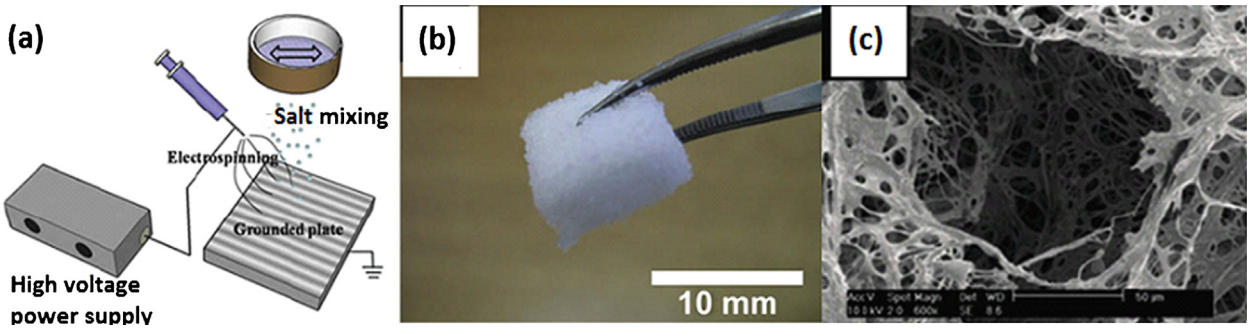

Fig. 10. Electrospinning concurrent with salt deposition: (a) schematic diagram of electrospinning and salt deposition set-up; (b) photograph of resultant nanofibers/salts composite. (c) SEM image of dried scaffold [108], Copyright 2008. Reproduced with permission from Elsevier Ltd.

Some of the aforementioned electrospinning techniques require the use of devices for some auxiliary processing. In fact, through controlling some parameters (e.g., the solution concentration/viscosity, electrostatic field, ambient humidity) during the conventional electrospinning process, a simple and rapid growth (or self-assembly) of 3D fibrous macro-structures has been achieved without any additional assistance. In this section, we briefly summarize the self-assembly of some typical electrospun 3D fibrous macro-structures such as fibrous honeycomb structure, nanofiber yarns, and fibrous stacks.

4.1. Honeycomb structure

Honeycomb structures have a mechanical stability for intersecting angle of 120° among the three branches. In nanoscience and technologies, 2D or 3D honeycomb structures are usually fabricated via breath figure templating method, patterning on unusual substrates (e.g., non-planar substrates, air/water interface), etc. [117–124]

Self-assembled electrospun nanofibrous structures with honeycomb-patterns were first reported by Deiztel et al. [58], when they utilized a precursor of PEO/water solution (7 wt%), and found a honeycomb-patterned structure, wet and full of bead defects, was prepared on a cloth substrate backed by an Al screen. However, when cotton and glass were used as collectors, the electrospun fibers were smooth-surfaced and without any bead defects, indicating that the high charge carrying beads are not solely responsible for the self-assembling process [125]. Furthermore, through fabricating well-defined 3D honeycomb-patterned structures based on PAN, PVA and PEO successfully (Fig. 11a), Yan et al. [116] found the concentration and humidity played important roles in the formation of these self-assembled 3D honeycomb-patterned structures. Namely, at a higher concentration (>3%), the self-assembly can not be observed and the electrospun products were randomly distributed dry nanofibers, while at a too low concentration (e.g., 1%), the electrospun products were solution droplets, which generally merge to form continuous 2D mats. Moreover, well-defined 3D honeycomb-patterned structures only form when the humidity (RH) is decreased below a certain level. If the humidity is higher than the limit, the self-assembled fiber clusters cannot grow high into the 3D walls although the self-assembling phenomenon can still be observed. Apart from the concentration and humidity, it is believed that the surface tension and electrostatic repulsion may be the key factor. As shown in Fig. 11b, when two or more wet as-spun nanofibers cross or contact each other at certain point, the surface tension may drive the segments near the contacting point to merge together, while the electrostatic repulsion tries to push them away from each other, resulting in the formation of partially overlapped fiber clusters. With the nanofibers merging, the charge density on the fiber clusters increases and therefore the electrostatic repulsion to the incoming nanofibers increases. When the nanofibers land and subsequently touch the fiber clusters, the surface tension may drive the part near the contacting position to incorporate into the clusters while the adjacent section farther away from the contacting point may be bent outward by the increased electrostatic repulsion. Simultaneously, the fiber clusters will be bent reversely, forming the branched structures. Driven by the electrostatic repulsion, the depositing nanofibers try to land on or move toward the positions with less charge to make the merged clusters similar in size. Because the mechanical stability can be most easily achieved for the three-branched structure with an intersecting angle of 120°, the nanofibers tend to form the networks composed of three-branched clusters. And the landing nanofibers captured by the clusters are pushed upward by the electrostatic repulsion, making the clusters grow high into the walls of the 3D honeycomb-patterned structures. This model was verified by their experimental results. However, no further experimental results to test whether the as-spun fibers on the collector are neutral or charged.

4.2. Nanofiber yarns

Nanofiber yarns can be regarded as special 3D fibrous assemblies. Single nanofibers with a small diameter have low mechanical strength and are difficult to tailor into a fibrous structure, restricting their further applications in some areas, such as high performance clothing, filters and composites. After precise handling of linear nanofiber

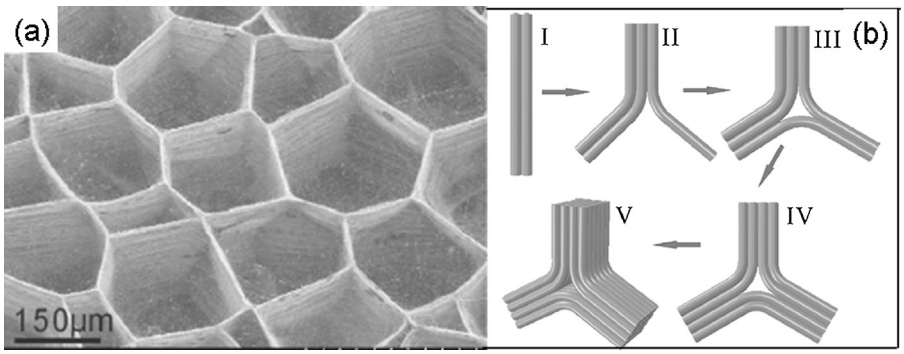

Fig. 11. (a) SEM image of well-defined self-assembled 3D honeycomb-patterned fibrous structures from PVA. (b) Schematic of the self-assembling mechanism of the electrospun honeycomb-patterned fibrous structures [116], Copyright 2011. Reproduced with permission from the American Chemical Society.

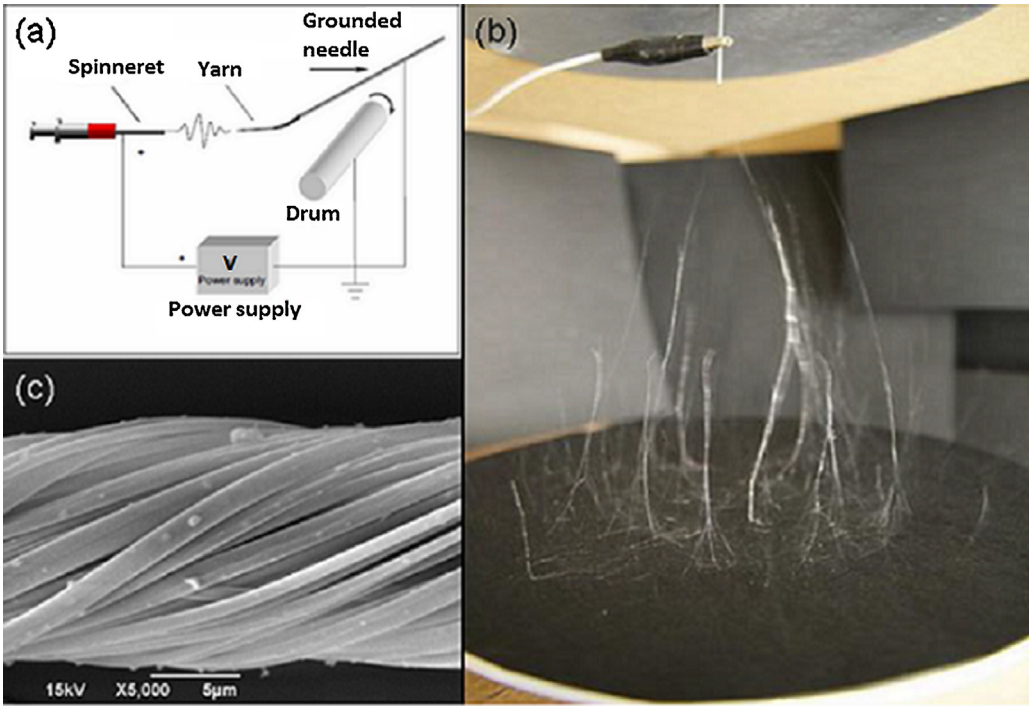

Fig. 12. (a) Schematic diagram of an electrospinning setup with a rotating collector for polymer fiber yarn manufacture [129], Copyright 2008. Reproduced with permission from Elsevier Ltd; (b) Photographs of spontaneous yarn formation from fibers prepared by electrospinning of chitosan/PAMPS/$CaCl_2$ solutions [135], Copyright 2010. Reproduced with permission from Elsevier Ltd; (c) SEM image of twist yarns of PVP fabricated by our group.

assemblies, nanofiber yarns can be used directly in weaving, knitting and embroidery.

As special 3D fibrous assemblies, fibers and yarns have a long history of thousands of years. With the development of nanoscience and technology, nanofibrous yarns based on various materials such as polymers, composites have created an increasing use in high value-added applications like filtration media, gas separation, sensors and biomedical engineering [126]. The fabrication of electrospun nanofiber yarns is usually based on a modified collector such as a water collector [83,84,127], a rotating drum (Fig. 12a) [128–131], and then the as-spun nanofibers were stretched manually or winded around the rotating grounded drum. The self-assembly of nanofiber yarns was first reported by Okuzaki et al. [132], where they observed that centimeters-long poly(p-phenylenevinylene) (PPV) nanofibers were spontaneously electrospun into yarns vertically (paralleling to the electric field) on the surface of a grounded collector (Al foil). Futhermore, with the presence of some low molecular weight salts (e.g., $CaCl_2$, NaCl, LiCl, $Fe(NO_3)_3$), the formation of self-assembled nanofibrous yarns can also be realized based on cellulose, PVP, chitosan/poly(2-acrylamido-2-methylpropanesulfonic acid) (PAMPS), etc. [133–135]. Fig. 12b shows the nanofiber yarns during electrospinning of chitosan/PAMPS/$CaCl_2$. The presence of the low molecular weight salt in the spinning solutions was considered as the main prerequisite for initiation of the self-organization process and the diameter of the yarns depended on the salt concentration [135]. Namely, the aforementioned phenomenon of self-assembly is thought to happen only to polymer solutions with high electrical conductivity because the conductive nature plays a key role in the formation of nanofiber yarns. The deposited precursor fibers discharge through polyelectrolyte chains to the grounded target, which prefers the following deposition on the fibers so as to decrease the distance between the fibers and the needle. Once a yarn is formed by touching the adjacent fibers swinging under the instable jet, the following deposition may occur preferably on the yarn rather than on the individual fibers. An electrostatic attractive force stretches the yarn vertically on the target electrode, leading to a successive upward growth of the yarn [132].

Generally, the self-assembly nanofibrous yarns are not such stable, and a subsequently collapse occurs once the high electrical field is removed, which restricts their use in practices. However, after precise handling of by weaving, knitting, or other embroidery processes, nanofiber yarns can be utilized not only for mechanical property enhancement, but also for scaffold fabrics, drug release, distributed sensors, electronic interconnects, electromagnetic shields, antennas and batteries [136–139]. Fig. 12c shows SEM image of twist yarns of PVP prepared by our group, with a smooth surface and improved mechanical properties, it may have potential application in microropes.

4.3. Fibrous stacks

The self-assembled 3D fibrous stack structures was first reported by Li et al. [134], prepared from PVP/$M(NO_3)_x$($M(NO_3)_x = Fe(NO_3)_3 + Co(NO_3)_2 + Ni(NO_3)_2$, and $Fe(NO_3)_3$: $Co(NO_3)_2$: $Ni(NO_3)_2$ = 1:1:1 by weight)

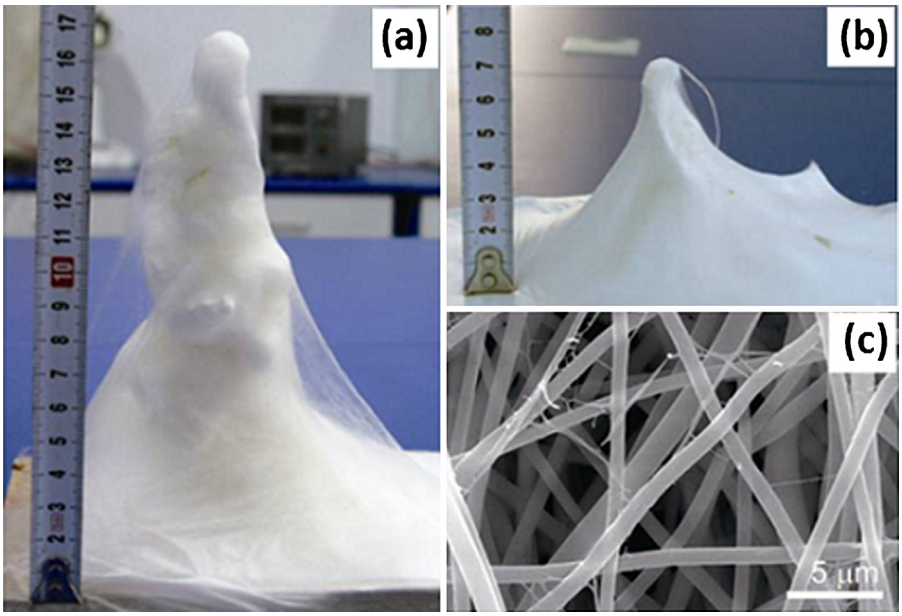

Fig. 13. (a) and (b) Self-assembled 3D fibrous stacks; (c) SEM image of (a) [134], Copyright 2011. Reproduced with permission from Trans Tech Publications.

solution. The fibrous stacks, with a height close to 10 cm (Fig. 13a and b), look as soft as silk and cotton, while their hardness increases after a while due to the evaporation of the solvent. All the fibers in stacks are uniform, similar to those of nonwoven mats fabricated by conventional electrospinning, as shown in Fig. 13c. Apart from PVP/M$(NO_3)_x$, pure polystyrene (PS) solution and PS/M$(NO_3)_x$ are both suitable for fabrication of self-assembled 3D fibrous stacks [140]. Meanwhile, Bonino et al. [141] also fabricated the same stack structure. By electrospinning an aqueous alginate-PEO-Pluronic F127 blend (10.6:0.8:1.5 wt%) for 40 minutes (0.5 mL h^{-1}) at 23 °C and 30% relative humidity, A fibrous stack appeared extending about 7 cm off the surface of the collector plate toward the needle.

Besides the rapid solidification of as-spun long fibers during the electrospinning process, electrostatic induction is believed to be the main factor for the formation of self-assembled 3D fibrous stacks: Firstly, the polymer jets ejected from the metal needle are positively charged due to the applied high dc voltages. After the process of fluid extension, whipping and splitting, and the evaporation of solvent, the spun fibers deposit on the grounded collector and the surface charges are conducted away through the Al foil. Then, due to electrostatic induction and polarization under the influence of strong static electric field, the as-spun fibers on the collector are negatively charged. Hence, during the electrospinning process, with the rapid increase in the amount of spun fibers, a piece of thin membrane appears on the collector. The observation that some regions of the fibrous membranes are not smooth and thicker at microscopic scale suggests that the polymer fibers may be polarized under a strong electric field. Negative charges generated by static induction and polarization on the top fibers will attract the coming jets/fibers with positive charges. Namely, the stack acts as a new "collector" in this case, the coming fibers deposit on the top of stack and make the stack grow fast within a short time [140]. In addition, the formation of 3D fibrous stacks also has relationship with the relative humidity. By changing the humidity of the electrospinning conditions, the concentration of dissociated ions in the fibers has been altered, which affects the like-charge repulsions between fibers and drives the 3D mat formation.

Accordingly, conversion between 3D fiber stacks and 2D thin film can be realized. With an insulating lucite plate placed over the Al foil collector during electrospinning the fibers would fully spread on the plate, forming a 2D nonwoven mat since the insulating lucite plate blocked dissipation of the positive charge on the fibers conducting through the ground wire. The fibers with positive charges on the lucite plate are no longer attractive to the spinning needle, on the contrary, repelling to the coming fibers with positive charges. Furthermore, when an additional electrostatic generator was introduced in the subsequent experiment, the conversion from 2D thin film to 3D fiber stack on the lucite plate can be achieved because the electrostatic generator generates enough negative charges. And the new fiber stack is almost the same as that without lucite plate and electrostatic generator, as shown in Fig. 14 [140].

4.4. Other methods

Apart from the conventional electrospinning, melt electrospinning can also lead to a self-assembled 3D fibrous macro-structure [142]. Fig. 15a demonstrates an electrospun boxlike structure depending on similar amount of fibrous layers stacked directly on top of each other with precise control with a thickness of approximately 1 mm, where electrostatic effects cause a loss of control over fiber deposition. Fig. 15b shows a combination of interweaving and fusion between the fibers in Fig. 15a, which may improve the structural integrity of melt electrospun

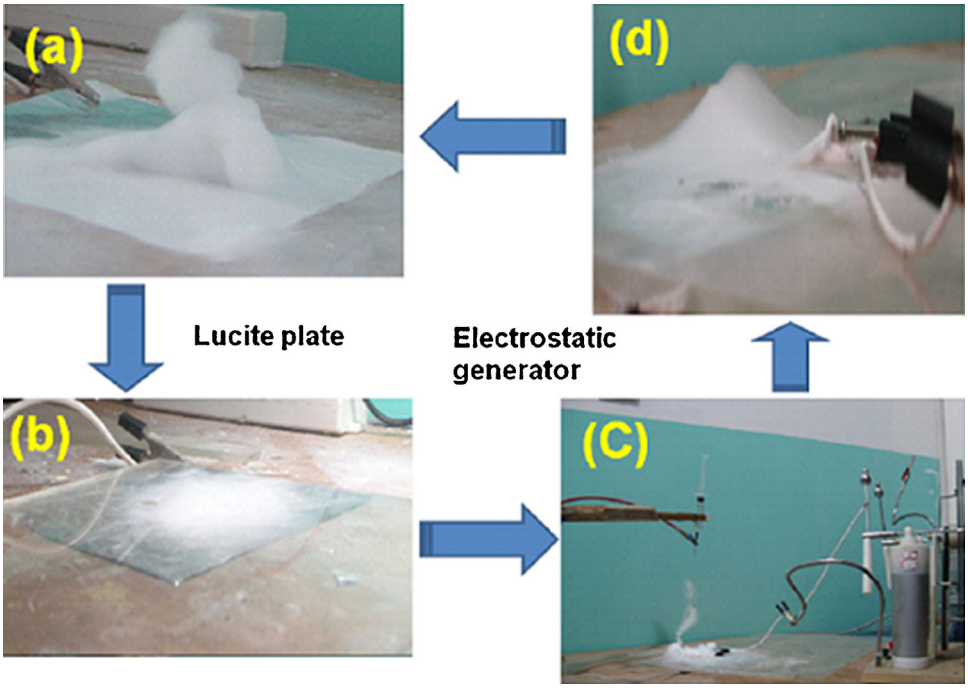

Fig. 14. Conversion between 3D fiber stack and 2D thin film: (a) 3D stack on an Al foil; (b) 2D fiber mat on a lucite plate; (c) the 2D mat is connected with an electrostatic generator; (d) 3D stack grown on the lucite plate [140], Copyright 2012. Reproduced with permission from the Royal Society of Chemistry.

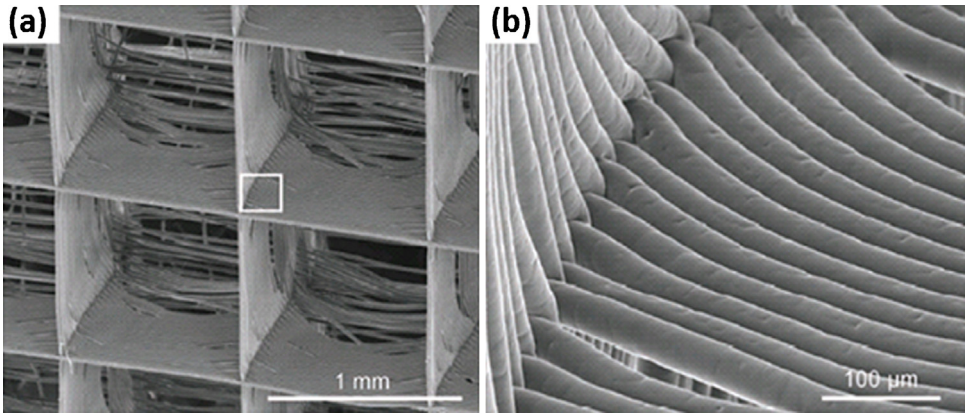

Fig. 15. SEM images of (a) the stacking and (b) interweaving of fibers to form an array of 1 mm × 1 mm × 1 mm boxes [142], Copyright 2011. Reproduced with permission from Wiley-VCH Verlag GmbH & Co, KGaA.

scaffolds. However, because material parameters such as polymer molecular weight and molecular chain conformation are important in all polymer fiber spinning methods, so it can be seen that the fibers' diameter in Fig. 15 is much larger than that from conventional solution electrospinning because of the stronger chain entanglement, higher viscosity and poor crystallization of the melt [143,144].

In addition, Shabani et al. [145] introduced a novel method to fabricate 3D nanofibrous scaffolds by using an array of focused halogen light bulbs, to localize the heat in the path of electrospun jet near the collector. It can be seen that the mat thickness from this method is ten times that from the conventional electrospinning, and the as-spun nanofibers much more porous than those fabricated by conventional electrospinning. It is potential to provide a suitable environment for viable cells to proliferate and migrate, and maybe appropriate for tissue engineering applications while enables researchers to fabricate 3D artificial tissues containing biodegradable polymers and functional cells.

In summary, each of the established electrospinning approaches possesses advantages and disadvantages, which have been summarized in Table 3.

5. Applications

Compared with the conventional electrospun 2D mats, 3D fibrous macro-structures have larger inner surface area and pore size, and thus improved cellular infiltration. It has been reported that cells can migrate up to approximately

Table 3
Summary of electrospinning technologies for assembling 3D fibrous macro-structures.

Electro-spinning technology	Advantages	Disadvantages	Examples	References
Multilayer electrospinning	Controlling of fiber diameter, composition, porosity of each layer and the total layer number	Time-consuming process	PCL, cellulose acetate, and PCL/β-TCP	[70–73]
Post-processing	Tthe as-spun mats can be tailored into desired patterns	A large space or distance between adjacent fibrous surfaces	Chitosan, PLLA, PLGA, PLGA/HAp, and PCL	[74–80]
Liquid-assisted collection	A larger pore size than that of 2D mats	An additional molding and freezing process usually required	PCL, PLGA, PGA, and PLLA/vaterite	[85–90]
Template-assisted collection	3D structures with same or different sizes, shapes, structures and patterns can be assembled.	A hybrid technique is usually needed	PCL, PDLLA, HAp/PVP, PLA, PLGA, and PLGA/TCP	[92–105]
Adding porogen	Structures with macropores be obtained	Porogen must be washed away or dried	Collagen	[108]
Self assembly	Only a traditional electrospinning device is used without any additional help	Hard to control the morphology, stability of the as prepared products	PEO, PVA, PAN, PPV, Cellulose, PVP, Chitosan/PAMPS, and PS	[58,116,132–135,140,141]
Other methods			PCL, PLLA	[142–145]

4 mm and showed a spatial cell distribution. [70,107] These physical and spatial architectural geometries, as well as the excellent biocompatibility of electrospun 3D scaffolds are important to applications in tissue engineering, such as nerve regeneration, vascular grafts, and bone regeneration, etc. Besides tissue engineering applications, 3D nanofibrous structures made of inorganic compound or composites may be also used as energy harvesting and storage materials such as cathode materials for solar cells and Li-ions batteries. In this section, these possible applications will be briefly introduced.

5.1. Tissue engineering

5.1.1. Guidance of cell outgrowth and nerve regeneration

Previous studies have demonstrated that 3D micro-/nanofibrous scaffold can improve cell attachment and spreading significantly due to surficial nanotopography and an enlarged inner surface of the structure. [103,104] In particular, 3D scaffold with oriented fibers or microgrooves could induce a uniform cell alignment as well as directional cell migration, and even guide the cell outgrowth [77,93,96]. For example, Badrossamay et al. [93] found that neonatal rat ventricular cardiomyocytes used the aligned rotary-jet-spun poly(lactic acid) (PLA) fibers to orient their contractile cytoskeleton and to self-organize into a beating, multicellular tissue that mimics the laminar, anisotropic architecture of the heart muscle. Uttayarat et al. [96] evaluated endothelial cell orientation on the luminal surface of small-diameter (~4 mm inner diameter and ~190 μm wall thickness) polyurethane (PU) grafts with microfiber and microgrooves. It was found that endothelial cells seeded onto the grafts formed confluent monolayers with individual cells exhibiting elongated morphology parallel to the direction of microgrooves and microfibers. Furthermore, the efficacy of oriented chitosan nanofibers on Schwann cell alignment and positive effect of chitosan nanofiber mesh tube on peripheral nerve regeneration were reported by Wang et al. [77] Fig. 16a shows that Schwann cells aligned in one same direction as a result of secure adhesion to the oriented fibers, and Fig. 16b exhibits that individual Schwann cells and their processes are capable to attach to single chitosan oriented fibers, although these cells sometimes continuously extend their processes to adjacent fibers. Histology of the regenerated nerve tissue in the implanted tube was also studied postoperatively after 30 weeks. As shown in Fig. 16c, the inner space of the tube in the oriented fiber group was well preserved to form regenerated nerve tissue resembling the isograft. Many myelinated axons with large diameters accompanied by Schwann cells had matured to mass on a large monofascicle in the oriented fiber group (Fig. 16d). For comparison, the regenerated nerve was still immature in the non-oriented fiber group. The results indicate that the oriented chitosan nanofiber mesh tube may be a promising substitute for autogenous nerve graft.

In addition, after precise handling of by weaving, knitting, nanofiber yarns can also be utilized in these applications. For example, woven PCL nanofiber fabric with interlacing warp (lengthwise) yarns and filling (crosswise) yarns at right angles have been fabricated by Khil et al. [138], the subsequently growth characteristics of mammary carcinoma cell (MCF-7) in these woven fabrics showed an important role of porous matrices for proliferation. And it may also have the potential to accommodate different types of cells for various applications in medical areas.

5.1.2. Vascular grafts

The small diameter bilayered or multilayered 3D nanofibrous tubular scaffolds especially with controllable nanofiber orientations have potential application in vascular grafts, because they not only have directional mechanical properties, but also can facilitate the orientation of the cell attachment on the fibers. [94,96,97,146] For example, Wang et al. [94] have demonstrated that

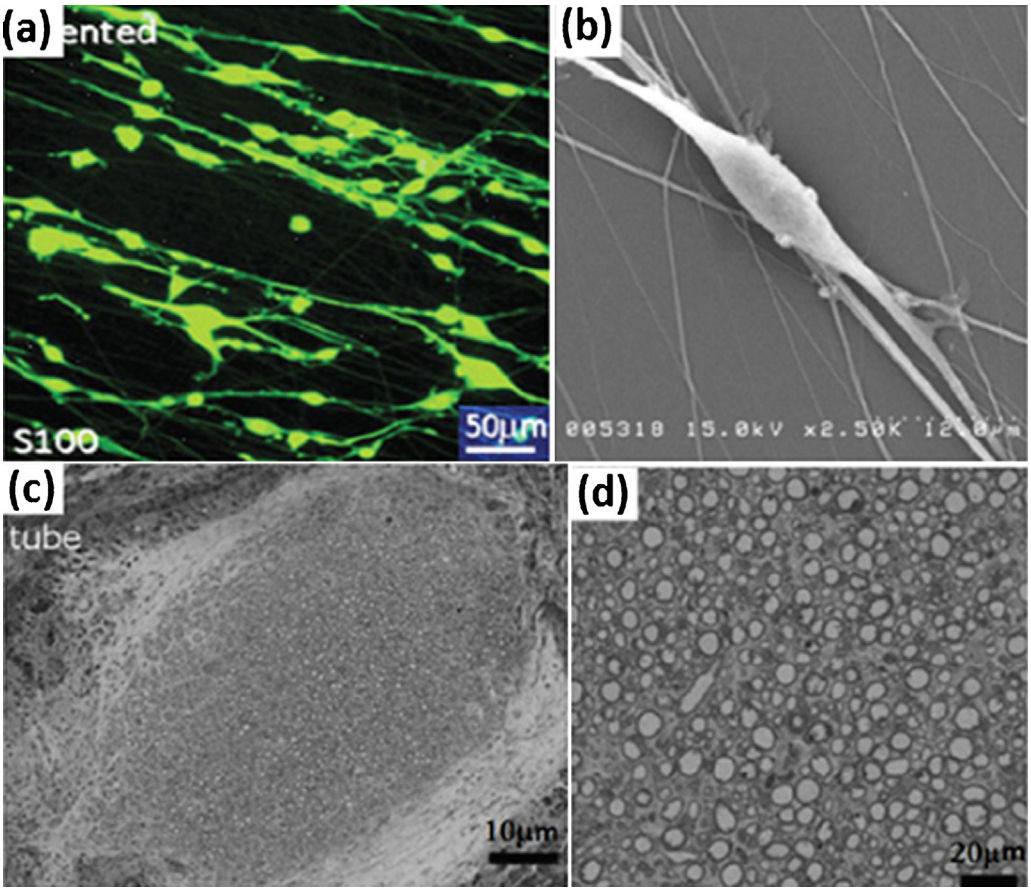

Fig. 16. (a) Immunocytochemistry of the immortalized Schwann cell line, IMS32 cultured for 4 days on coverslip coated with oriented chitosan nanofibers. (b) SEM image of Schwann cells cultured on the oriented chitosan nanofiber mesh sheet. (c) Histology of the grafted tube harvested at 30 weeks after implantation. The inner space of the tube in the oriented fiber group was preserved well, forming regenerated nerve resembling the isograft. (d) Higher magnification of the regenerated nerves in the chitosan tube observed in (c). Many large diameter myelinated axons have matured to mass in the oriented fiber group [77], Copyright 2009. Reproduced with permission from Wiley-VCH Verlag GmbH & Co, KGaA.

tubular scaffold (a length of 40 mm and an inner diameter of 4.5 mm with a thickness of 0.5 mm, as shown in Fig. 17a) composed of polylactide fibers (outside layer) and silk fibroin-gelatin fibers (inner layer), which was fabricated by multi-electrospinning using a rotating mandrel-type collector, can be considered as an ideal candidate for tissue engineering blood vessel. It was found that the polylactide/silk fibroin-gelatin (PLA/SF-gelatin) composite tubular scaffolds, with porosity of approximately $82 \pm 2\%$, possessed appropriate breaking strength (2.21 ± 0.18 MPa), pliability ($60.58 \pm 1.23\%$), and suture retention strength (4.58 ± 0.62 N). In addition, the burst pressure strength of the tubular scaffolds reached 1596 ± 20 mmHg. These biomechanical properties results indicate the composite tubular scaffolds possess adequate strength to develop as a substitute for native blood vessels. Moreover, the composite scaffolds could hardly dissolve in the water, the water-dissolved rate was only $0.3 \pm 0.1\%$. Mitochondrial metabolic (MTT) activity assay and cell morphology observation indicated that both 3T3 mouse fibroblasts (Fig. 17b) and human umbilical vein endothelial cells (HUVECs) (Fig. 17c and d) could adhere, spread, and proliferate well on the composite tubular scaffolds after culturing for 14 and 21 days, respectively. As shown in Fig. 17b, cell proliferation on the composite scaffolds were higher than controls, indicating the 3D scaffolds, having high surface area to volume ratio and porosity, were more suitable for cell growth than the culture dish with smooth surface. The SEM images shown in Fig. 17c and d exhibited that at day 7, only a few cells could be observed on the scaffolds; at day 14 there was an increase in cell densities compared to day 7, and the cells were also observed to migrate and proliferate in certain patterns, forming a continuous monolayer. The subcutaneous implantation results are also shown in Fig. 17e–g. It can be seen that electrospun PLA/SF-gelatin scaffolds were surrounded by the new tissue after implantation of months 1 and 2, and macrophages and lymphocytes were not observed, indicating that the composite scaffolds could induce minor inflammatory reactions in vivo. At month 3 the scaffolds could guide the formation of connective vascular network. The shape of implants became smaller, suggesting that the scaffolds had good biocompatibility and can be biodegraded gradually in vivo. All the investigations demonstrate that the composite tubular scaffolds are appropriate candidates for vascular grafts. Similar results have also been observed

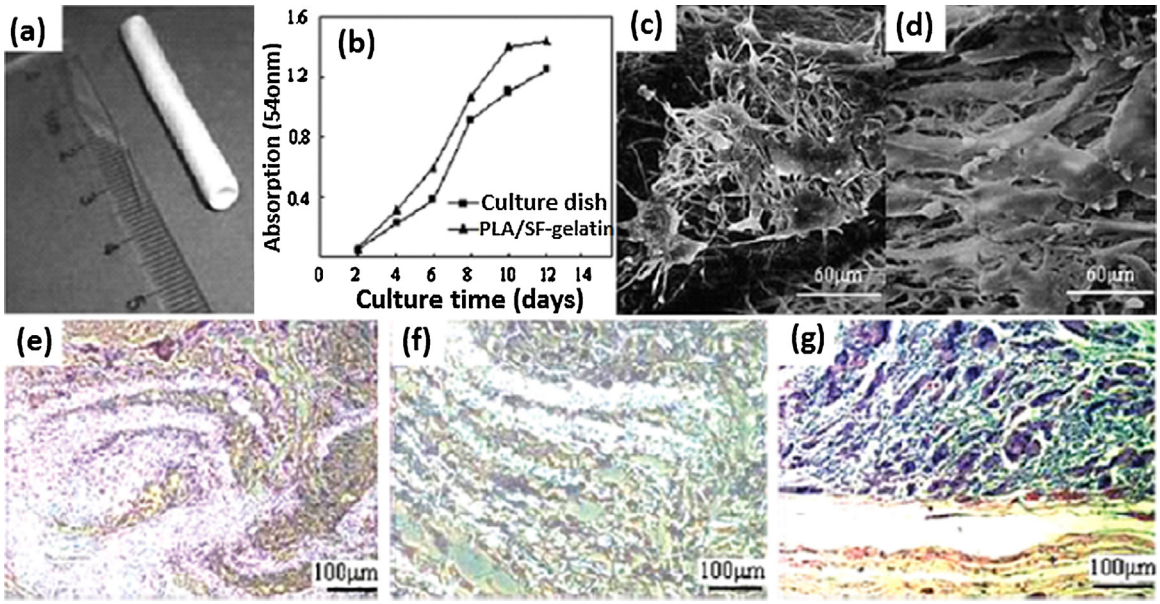

Fig. 17. (a) Macroscopic view of the PLA/SF-gelatin composite tubular scaffold. (b) Growth and proliferation of 3T3 mouse fibroblast on the tubular scaffold and culture dish (for comparison). (c and d) SEM images of human umbilical vein endothelial cells seeded on the tubular scaffolds after 7 and 14 days of culture, respectively. (e–g) Representative histological photomicrographs of the subcutaneous implants: PLA/SF-gelatin at 1, 2, and 3 months, respectively [94], Copyright 2009. Reproduced with permission from the American Chemical Society.

by Soletti et al. [147]. In their work, a composite scaffold incorporating a highly porous poly(ester-urethane)urea (PEUU) inner layer and an external electrospun nanofiber layer was prepared for small diameter vascular grafts. The mechanical properties of the bilayered scaffold were comparable with native vessels, and the combination of the two layers enabled better cell integration and growth. Because of the porosity difference in the two layers, high cellular density was found in the inner layer.

5.1.3. Bone regeneration

Another interesting application of 3D fibrous scaffolds is bone tissue engineering, which has been reported by several research groups in recent years. [74,78,99,101] For example, Shim et al. [74] fabricated poly(L-lactic acid) (PLLA) microfibrous scaffolds with 3D structures by an electrospinning technique with a subsequent mechanical expansion process, and found that microfibrous matrices were a favorable substrate for cell infiltration and bone formation after 2 and 4 weeks, using a rabbit calvarial defect model. Cai et al. [78] also reported a novel electrospinning-based yarn assembly technique to create 3D macroporous nanofibrous PLLA/PCL (w/w 9:1) scaffold with 3 mm in thickness and 15 mm in diameter, which possessed good mechanical strength (elastic modulus was 71.68 ± 5.61 MPa) as well as sufficient interconnected micropores (porosity was 77.61 ± 6.35%). The efficacy of the 3D scaffold for bone formation was evaluated using human embryonic stem cell-derived mesenchymal stem cells differentiation model and rabbit tibia bone defect model. In vitro more cell proliferation and cell ingrowth were observed in the 3D scaffold. In vivo the 3D scaffold treated bone defect had fine 3D bony tissue formation around the scaffold as well as inside the scaffold at 3 weeks and 6 weeks. As shown in Fig. 18a and b, at 3 weeks, obvious cell infiltration and new bone-like tissue were observed both at the central part of the scaffold and at the marginal region, and new extracellular matrix was almost filled with the whole scaffold. At week 6, much thicker and more mature bony tissue was found in most regions of the scaffold, and the newly formed cortical bone was interconnected and acted as a structural and functional unit (Fig. 18c and d).

In addition, Schneider et al. [99] reported the in vitro and in vivo performance of a flexible, moldable, cotton-like nanocomposite based on poly(lactide-*co*-glycolide) and amorphous tricalcium phosphate nanoparticles (PLGA/TCP, w/w 60:40) as bone graft substitute material. The 3D PLGA/TCP scaffolds were fabricated by a low-temperature electrospinning with a rotating collection drum loaded with dry ice. Bone regeneration was quantitatively investigated by creating four circular (diameter = 6 mm) non-critical-size calvarial defects in New Zealand white rabbits. The effects were filled with the cotton-like PLGA/TCP fibers or PLGA alone. For comparison, porous bovine-derived mineral (Bio-Oss©, today's "gold standard" for bone regeneration) was used as a positive control, and cavities left empty served as a negative control. As shown in Fig. 18e and f, the micro-computed tomographic (μCT) analysis indicated that after 4 weeks implantation, the average area fraction of newly formed bone was significantly increased for tricalcium phosphate-containing PLGA/TCP fibers compared to pure PLGA. A spongiosa-like structure of the newly formed bone tissue was observed for PLGA/TCP nanocomposites, whereas Bio-Oss©- treated defects afforded a solid cortical bone. These results indicate that the flexible, mouldable and highly bioactive calcium phosphate/PLGA nanocomposite can be

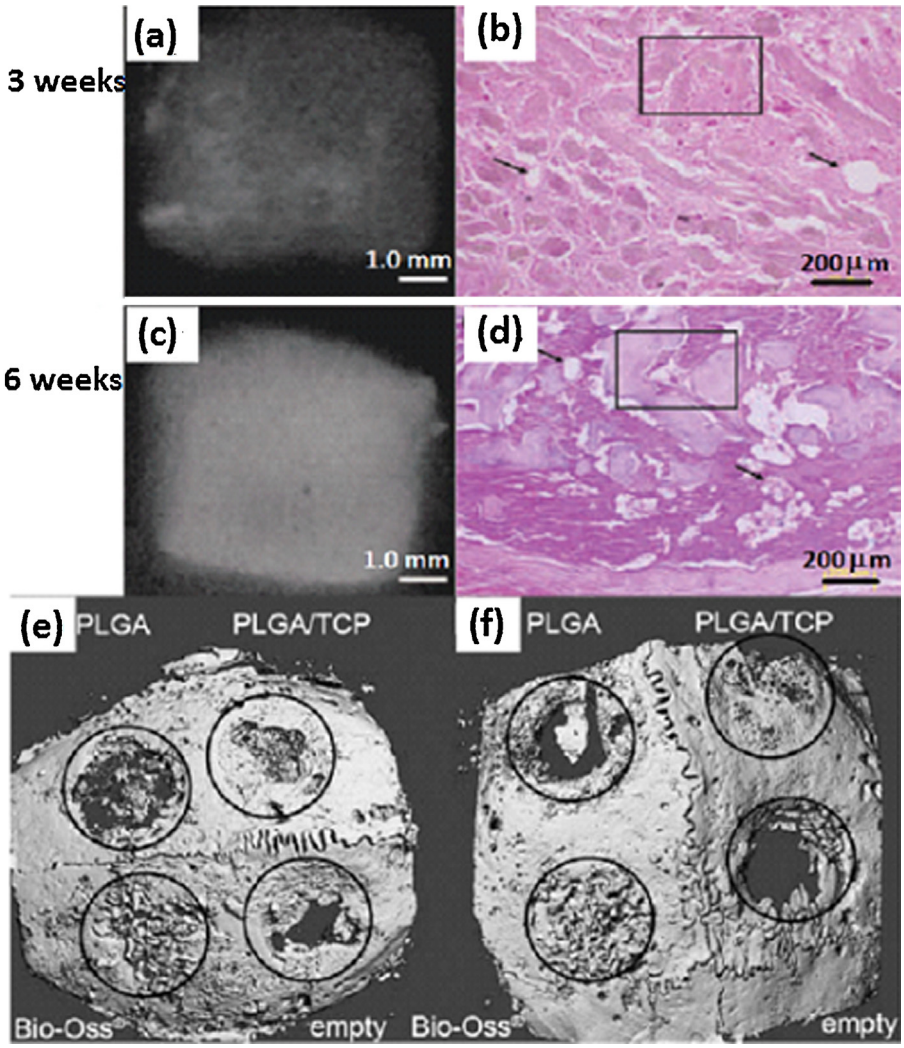

Fig. 18. (a and c) Representative radiographs of implanted PLLA/PCL scaffolds at 3 and 6 weeks, respectively. (b and d) Representative photomicrographs of implanted PLLA/PCL scaffolds at 3 and 6 weeks, respectively. Black arrow indicates blood vessel [78], Copyright 2012. Reproduced with permission from Wiley-VCH Verlag GmbH & Co, KGaA. (e and f) Two examples of the micro-computed tomography of the entire cranial bone are shown. Defect margins and treatment modalities (PLGA, PLGA/TCP, Bio-Oss© and empty) are indicated [99], Copyright 2009. Reproduced with permission from Elsevier Ltd.

used as a highly porous bone regeneration scaffold for complex defects.

Furthermore, the strategies for improved drug loading and functionalization of electrospun fibers, the influence of the pore size and fiber diameter of the as-spun 3D fibrous macro-structures, and the drug release kinetics have been reviewed recently [148].

5.1.4. Skin tissue engineering

Considering that the two layers of skin, epidermis and dermis, have different ability to regenerate: the epidermis has less capacity to heal; however while the dermis has an enormous capacity to regenerate [149], skin tissue engineering should be not only to close the skin wound but also to stimulate the regeneration of the dermis. Nanofibers reveal fascinating potential in this area due to their structural similarity to the extracellular matrix (ECM), large surface-area-to-volume ratio, superior mechanical properties, and high porosity. Apart from natural polymers (e.g., Xylan, chitosan, gelatin, collagen, silk fibroin), several synthetic polymers (e.g., poly (3-hydroxybutyrate-co-3-hydroxyvalerate) (PHBV), poly(lactic acid-*co*-glycolic acid) (PLAGA), PLGA, poly(L-lactic acid)-*co*-poly(3-caprolactone) (PLLCL), PCL, etc.) as nanofibrous macro-structures, have been explored for skin tissue engineering [150–157]. For example, electrospun 3D PLAGA matrices with various fiber diameters demonstrated a tensile modulus from 39.23 ± 8.15 to 79.21 ± 13.71 MPa, in the range for normal human skin. Analysis of the dependence on fiber diameter showed that human skin fibroblast seeded in the matrices with fiber diameter range of 350–1100 nm revealed significantly higher proliferation rate than the fiber matrices below and beyond this range, leading to a well spread morphology and formed cell multilayers on the scaffolds after 28 days in culture [151]. Recently, Xylan was electrospun along with polyvinyl alcohol (PVA)

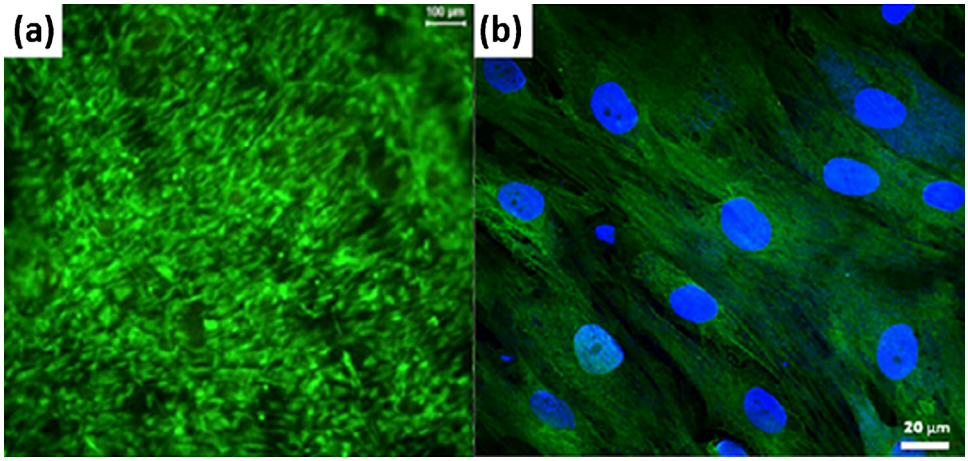

Fig. 19. (a) Morphology of cultured fibroblasts on day 15 in the Xylan/PVA scaffolds [152], Copyright 2012. Reproduced with permission from Springer-Verlag; (b) Laser scanning confocal microscope images of MSC grown in normal growth medium on collagen/PLLCL nanofibers stained with Ker 10, after 15 days cell culture [155], Copyright 2012. Reproduced with permission from Wiley-VCH Verlag GmbH & Co, KGaA.

to produce Xylan/PVA 3D nanofibrous structures for skin tissue engineering [152]. The Xylan/PVA nanofibrous scaffolds have a rough surface that was desirable for better cell attachment, growth and proliferation and also enhanced by the presence of functional groups and surface hydrophilicity. Human foreskin fibroblasts showed a good morphology and even distribution after 15 day's cultured in the scaffolds, as shown in Fig. 19a. In addition, nanofibrous scaffolds based on electrospun collagen/PLLCL were adopted to mimic the fibrous structure of native skin ECM for epidermal differentiation of mesenchymal stem cells (MSC). The proliferation of MSC evaluated by cell proliferation assay suggested that the number of cells grown on collagen/PLLCL nanofibrous scaffolds was significantly higher than those on PLLCL scaffolds; Fig. 19b shows MSC grown in normal growth medium on collagen/PLLCL nanofibers after 15 days cell culture [155].

5.2. Energy harvest and storage materials

In addition to the tissue engineering applications described in the preceding, 3D nanofibrous structures made of inorganic compounds or composites also have potential applications in energy harvest materials, such as cathode materials for Li-ions batteries and solar cells. For example, Dimesso et al. [158] reported that 3D structures of $LiFePO_4$-coated carbon nanofiber nonwovens can be used as the cathode material of Li-ion batteries. The nonwoven mats from carbon black nanoparticles-polyacrylonitrile (PAN) solutions were electrospun first, and then removed from the aluminum substrate and folded into small rectangular $1 \times 0.8\,cm^2$ pieces. After pressed, stabilized in air, and carbonized in nitrogen at 1050 °C for 30 min, the composites were cut into 5–7 mm diameter disks, 1–2 mm thick. The cathode materials were prepared by (1) soaking the 3D nonwovens in a starting aqueous solution containing lithium, iron, and phosphate ions at 80 °C; (2) after cooling down the solution, the prepared composites were rinsed slightly with water and dried by heating at 130 °C for 24 h in vacuum and finally annealed at 600 °C for 5 h. Surface investigation of the prepared materials revealed a uniform distribution of the $LiFePO_4$ crystalline phase over the surface area of the carbon nonwoven nanofibers, as shown in Fig. 20a. Electrochemical measurements on the $LiFePO_4$/carbon-nanofiber composites showed good performances delivering a discharge capacity of 156 and 152 $mAh\,g^{-1}$ at discharge rates of C/25 and C/10 at room temperature, respectively (Fig. 20b). This specific capacity of the composites corresponds to the 92% of the theoretical value (at C/25) and 89.5% (at C/10). The good electrochemical performances could be ascribed to a high electronic conductivity and a high "free" surface area of the carbon nanofibers.

In addition, dye sensitized solar cells (DSSCs) with vertical nanofibers of electrospun TiO_2 as a photoelectrode have been reported [4,159,160]. The aligned nanofibrous TiO_2 ribbons were firstly produced by electrospinning, and then erected to vertical nanofibers after post-treatment of rolling up, stacking and cutting with a 3D structure (Fig. 20c). The as-produced vertical ceramic TiO_2 nanowires array possessed an area of $0.2\,cm^2$, with nanowire diameter of 90 ± 30 nm, and height up to 27 μm. The advantage of this method is that the height of the vertical nanowires can be easily varied from 10 to 100 μm. The conversion efficiency, short circuit current, and open circuit voltage of the resultant DSSC were measured as 2.87% and 5.71 $mA\,cm^{-2}$, 0.782 V, respectively, as shown in Fig. 20d. Enhanced photo-conversion efficiency is very likely possible by using this method upon optimizing the height of the vertical nanowires, improving the porosity, and reducing the diameter.

5.3. Filtration

Electrospun nanofiber-based filters for industry, household and defense applications have a history of more than 20 years, because electrospun nanofiber mats provides dramatic increase in filtration efficiency at relatively small decrease in permeability. For example, Gibson et al. [161] revealed that electrospun nanofiber mats were extremely

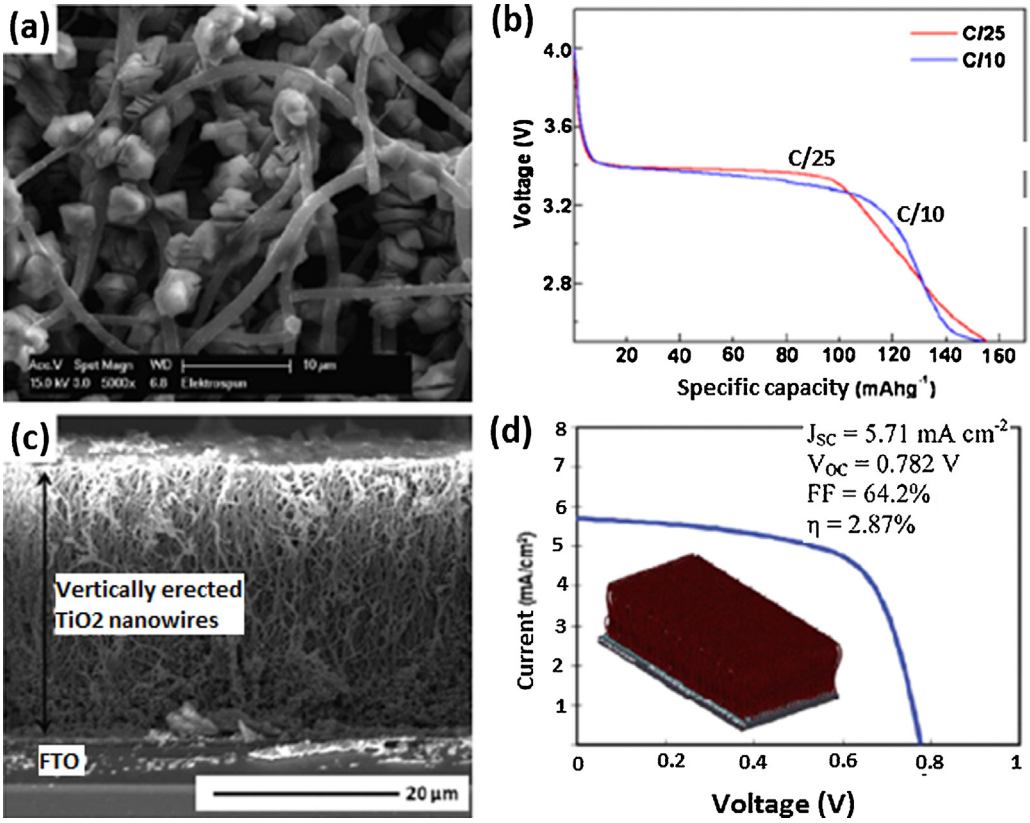

Fig. 20. (a) SEM image of the $LiFePO_4$/carbon-nanofiber composites prepared via a simple sol-gel process on electrospun carbonized nanofibers; (b) Voltage–capacity curves for the second discharging, measured at discharge rates of C/25 and C/10 and room temperature, for $LiFePO_4$/carbon-nanofiber composites [158], Copyright 2012. Reproduced with permission from the American Institute of Physics; (c) SEM image of vertically erected electrospun TiO_2 nanowires on an FTO plate for solar cell applications; (d) Photocurrent density versus voltage of a vertical anatase TiO_2 nanowires array electrode under AM 1.5 illumination [159], Copyright 2011. Reproduced with permission from the Royal Society of Chemistry.

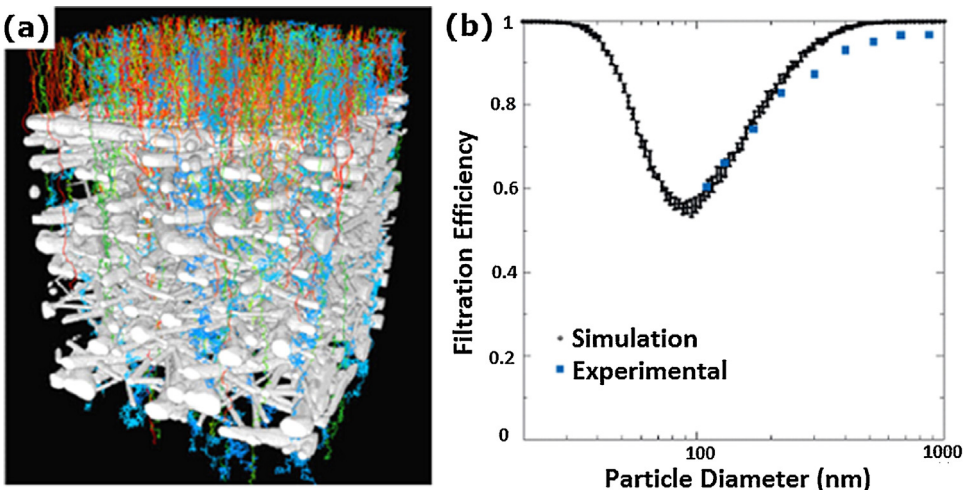

Fig. 21. (a) Flow path lines through 3D multilayered nonwoven nanofibrous medium colored by particle sizes (50 nm—blue, 200 nm—green, 500 nm—red); (b) Comparison between measured and predicted filtration efficiency curves for the polyurethane electrospinning nonwoven multilayered nanofibrous sample [164], Copyright 2011. Reproduced with permission from Elsevier Ltd. (For interpretation of the references to color in this figure legend, the reader is referred to the web version of the article.)

efficient at trapping airborne particles (0.5–200 μm). Barhate and Ramakrishna [162] reported that a nylon-6 electrospun nanofiber mat (thickness 100 μm, average pore size 0.24 μm) had a slightly higher filtration efficiency (99.993%) than a commercial high efficiency particle air filter (99.97%, thickness 500 um, average pore size 1.7 μm). In particular, it was recently reported that filters made of multiple thin nanofiber layers had a much better filtration performance than single thick layer nanofiber mat in terms of the pressure drop during filtration [163]. Furthermore, 3D modeling of filtration process via multilayered electrospun polyurethane (PU) nanofiber based nonwoven filters was also proposed [164], as shown in Fig. 21a. The obtained theoretical predictions for the filtration efficiency have been compared with the corresponding experimental data (Fig. 21b). It is obvious that particles with a wide range of diameters could be removed, but their filtration mechanisms are different. For large particles (>400 nm), they are blocked on the filter surface due to the sieve effect. For particles smaller than the surface-pores, they could still be collected by the fibers through a mechanism such as interception, impaction, or static electrical attraction. Very fine nanoparticles (<20 nm) could also be captured by the Brownian motion effect.

6. Challenges in electrospinning

Compared with other nanofiber fabrication processes, electrospinning is versatile and superior in production and construction of ordered or more complex nanofibrous assemblies. Although a lot of progress has been achieved in the past two decades in the development of various designs and modification to the electrospinning process and wide potential applications of electrospun fibers [165–175], there are still many areas that require further improvement and refinement, e.g., consistent production of nanofibers, controlling the fiber diameter and size distribution, reproducible placement of nanofibers in specific positions and orientations, mass production.

To fully explore the extraordinary number of application opportunities of electrospun nanofibers, reliable consistent production of the nanofibers especially at the industrial level is essential. Since the morphology and diameter of the electrospun nanofibers are dependent on material and processing parameters, through controlling these interrelated variables such as solution conductivity, spinneret design, electric field intensity, auxiliary electric/magnetic field, applied voltage, flow rate, collection distance, solution concentration, etc., the morphology, average diameter, diameter distribution, and orientation of the electrospun nanofibers can be controlled and adjustable. For example, Zhang et al. [68] examined the affect of conductivity of PVA/water solution on the diameters of electrospun fibers. By adding increasing concentrations of NaCl (ranging from 0.05 to 0.2%) to the PVA/water solution, the corresponding solution conductivity increased from 1.53 to 10.5 mS cm^{-1}, the average fiber diameter decreased from 214 to 159 nm, and the diameter distribution broadened. In another study, Niu et al. [176] examined the effects of the spinneret shape on the needle-less electrospinning process and resultant fiber morphology. It is found that compared to cylinder, the disk and coil produced thinner fibers with narrower diameter distribution, which could be ascribed to concentrated electric field formed on disk edge and coil wire surface. Liu et al. [177] also reported that PLGA fibers fabricated by magnetic-field-assisted electrospinning exhibited smaller diameter and narrower size distribution than those prepared by conventional electrospinning. In addition, nanofibers produced by nozzle-less electrospinning (Nanospider^{TM}, ELMARCO) have average diameters of 80, 100, 150, 200, 250 nm and higher with a standard deviation of typically ±30%, while the stand deviation of fibers via nozzle electrospinning tends to vary over fiber length [178].

Since the random orientation of fibrous mats fabricated by the conventional electrospinning may limit the potential applications of electrospun fibers, especially in the fields of electronics, photonics, photovoltaics, actuators and tissue engineering which need direct, fast charge transfer or regular, uniform structures. To solve this problem, a variety of strategies have been proposed by many research groups, such as pair electrodes collection, rotating drum or disk collection, auxiliary electric or magnetic electrospinning, double spinning, near-field electrospinning, direct-writing electrospinning, etc. Some approaches such as rotating drum collection have been used in the commercial electrospinning setup. However, a drum collector is not able to develop highly aligned fiber mesh with a large thickness due to electrostatic repulsion between the deposited fibers and the coming fibers. The ability to consistently fabricate highly aligned fibers in large quantity over a large area is still a challenge.

In particular, recent advances in near-field electrospinning (precision electrospinning or direct writing electrospinning) have demonstrated the ability to precisely control fiber deposition to form patterns [142,179–182]. By fixing the collector or spinneret on an X-Y motion stage, the movement of the collector/spinneret can be controlled in the pre-programmed track via a host computer, and thus precise fiber deposition and various complex patterns of polymer fibers with controlled orientation and spacing have been achieved, which is vital for device or biomedical applications [3,182]. However, the assembly efficiency and the pattern area need to be improved for practical use.

7. Summary and outlook

There are a variety of approaches for building 3D porous structures. In this paper, only recent advances in fabricating 3D fibrous macro-structures via electrospinning process have been reviewed, including some techniques such as multilayer electrospinning, post-processing of the as-spun fibers, using 3D collectors or liquid collectors. In particular, self-assembled 3D fibrous macro-structures by electrospinning are discussed in detail. It is interesting that the fibers in the 3D fibrous macro-structures are similar to those of 2D mats fabricated by conventional electrospinning, ranging from several micrometers down to tens of nanometers. For the large surface area and pore size and the existence of the inter-pore channels compared with the 2D mats, these 3D structures have potential applications in some fields such as tissue engineering, filtration, and

energy materials. And other potential applications may lie in catalyst supports, micro-containers, sensors, drug delivery, sound absorption, and so on.

Nevertheless, challenges in this area have also been met and many practical problems have to be solved. For example, several 3D fibrous materials such as self-assembled stacks and vertically aligned fibrous structures cannot be put in tissue engineering use directly due to their structure instability. These 3D nanofibrous macro-structures require post-processing for practical use. In order to improve the performance of 3D fibrous scaffolds in tissue engineering applications, besides optimizing the porosity, size scale and orientation of nanofibers, some other approaches such as surface functionalization of nanofibres with biological molecules [183–193] and electrospinning of polymers with bioactive inorganic nanoparticles or nanotubes/wires [194–198] may be effective. For example, surface modification of nanofibrous scaffolds with biological molecules such as gelatin [184], short peptide sequence Arg-Gly-Asp (RGD) [185,186], perlecan [187], acrylic acid [188], collagen [189], polydopamine [190,191], and protein [192] can be used to further enhance the interactions between cells and the scaffold material and improve their in vivo usage. Many studies on composite fibrous scaffolds containing bioactive inorganic nanoparticles such as hydroxyapatite (HA) and calcium phosphate have demonstrated enhanced in vitro attachment, differentiation and proliferation of bone forming cells, and in vivo bone regeneration [194–196]. In addition, since the engineering of complex tissues requires graded scaffolds that can mimick the complex spatial distributions of composition, structure, and functionality of native tissues, it is still a challenge to fabricate biodegradable 3D scaffolds functionally graded in terms of porosity and composition distributions.

Acknowledgments

This work was supported by the National Natural Science Foundation of China (Grant Nos. 11074138, 11004114), the Natural Science Foundation of Shandong Province, China for Distinguished Young Scholars (Grant No. JQ201103), the Taishan Scholars Program of Shandong Province, China, the National Key Basic Research Development Program of China (973 special preliminary study plan) (Grant No. 2012CB722705), the Project of Shandong Province Higher Educational Science and Technology Program (Grant No. J13LJ07) and the Program for Scientific Research Innovation Team in Colleges and Universities of Shandong Province, China.

References

[1] Xia YN, Yang P, Sun Y, Wu Y, Mayers B, Gates B, Yin Y, Kim F, Yan H. One-dimensional nanostructures: Synthesis, characterization, and applications. Advanced Materials 2003;15:353–89.
[2] Long YZ, Li MM, Gu CZ, Wan MX, Duvail JL, Liu ZW, Fan ZY. Recent advances in synthesis, physical properties and applications of conducting polymer nanotubes and nanofibers. Progress in Polymer Science 2011;36:1415–42.
[3] Long YZ, Yu M, Sun B, Gu CZ, Fan Z. Recent advances in large-scale assembly of semiconducting inorganic nanowires and nanofibers for electronics, sensors and photovoltaics. Chemical Society Reviews 2012;41:4560–80.
[4] Yu M, Long YZ, Sun B, Fan Z. Recent advances in solar cells based on one-dimensional nanostructure arrays. Nanoscale 2012;4:2783–96.
[5] Huang ZM, Zhang YZ, Kotaki M, Ramakrishna S. A review on polymer nanofibers by electrospinning and their applications in nanocomposites. Composites Science & Technology 2003;63:2223–53.
[6] Lu XF, Wang C, Wei Y. One-dimensional composite nanomaterials: synthesis by electrospinning and their applications. Small 2009;5:2349–70.
[7] Weintraub B, Wei Y, Wang ZL. Optical fiber/nanowire hybrid structures for efficient three-dimensional dye-sensitized solar cells. Angewandte Chemie International Edition 2009;121:9143–7.
[8] Langer R, Vacanti J. Tissue engineering. Science 1993;260:920–6.
[9] Lanza RP, Langer R, Vacanti J, editors. Principles of Tissue Engineering. second ed. New York: Academic Press; 2002. p. 995.
[10] Fang J, Niu H, Lin T, Wang X. Applications of electrospun nanofibers. Chinese Science Bulletin 2008;53:2265–86.
[11] Ng R, Zang R, Yang KK, Liu N, Yang ST. Three-dimensional fibrous scaffolds with microstructures and nanotextures for tissue engineering. RSC Advances 2012;2:10110–24.
[12] Yang Y, Basu S, Tomasko DL, Lee LJ, Yang ST. Fabrication of well-defined PLGA scaffolds using novel microembossing and carbon dioxide bonding. Biomaterials 2005;26:2585–94.
[13] Ma Z, Kyotani T, Liu Z, Terasaki O, Tomita A. Very high surface area microporous carbon with a three-dimensional nano-array structure: synthesis and its molecular structure. Chemistry of Materials 2001;13:4413–5.
[14] Pattison MA, Wurster S, Webster TJ, Haberstroh KM. Three-dimensional, nano-structured PLGA scaffolds for bladder tissue replacement applications. Biomaterials 2005;26:2491–500.
[15] Javey A, Nam WS, Friedman RS, Yan H, Lieber CM. Layer-by-layer assembly of nanowires for three-dimensional, multifunctional electronics. Nano Letters 2007;7:773–7.
[16] Guo SJ, Dong SJ, Wang EK. Three-dimensional Pt-on-Pd bimetallic nanodendrites supported on graphene nanosheet: Facile synthesis and used as an advanced nanoelectrocatalyst for methanol oxidation. ACS Nano 2010;4:547–55.
[17] Ovsianikov A, Malinauskas M, Schlie S, Chichkov B, Gittard S, Narayan R, Löbler M, Sternberg K, Schmitz KP, Haverich A. Three-dimensional laser micro- and nano-structuring of acrylated poly(ethylene glycol) materials and evaluation of their cytoxicity for tissue engineering applications. Acta Biomaterialia 2011;7:967–74.
[18] Guldin S, Hüttner S, Kolle M, Welland ME, Müller-Buschbaum P, Friend RH, Steiner U, Tétreault N. Dye-sensitized solar cell based on a three-dimensional photonic crystal. Nano Letters 2010;10:2303–9.
[19] Mikos AG, Bao Y, Cima LG, Ingber DE, Vacanti JP, Langer R. Preparation of poly(glycolic acid) bonded fiber structures for cell attachment and transplantation. Journal of Biomedical Material Research 1993;27:183–9.
[20] Zhang K, Wang X, Jing D, Yang Y, Zhu M. Bionic electrospun ultrafine fibrous poly(L-lactic acid) scaffolds with a multi-scale structure. Biomedical Materials 2009;4, 035004/1-6.
[21] O'Brien FJ, Harley BA, Yannas IV, Gibson LJ. The effect of pore size on cell adhesion in collagen-GAG scaffolds. Biomaterials 2005;26:433–41.
[22] Lam CXF, Mo XM, Teoh SH, Hutmacher DW. Scaffold development using 3D printing with a starch-based polymer. Materials Science and Engineering: C 2002;20:49–56.
[23] Yang S, Leong KF, Du Z, Chua CK. The design of scaffolds for use in tissue engineering. Part I. Traditional factors. Tissue Engineering 2001;7:679–89.
[24] Teo WE, Inai R, Ramakrishna S. Technological advances in electrospinning of nanofibers. Science & Technology of Advanced Materials 2011;12, 013002/1-19.
[25] Li MM, Long YZ, Yang DY, Sun J, Yin H, Zhao Z, Kong W, Jiang XY, Fan ZY. Fabrication of one dimensional superfine polymer fibers by double-spinning. Journal of Materials Chemistry 2011;21:13159–62.
[26] Teo WE, Ramakrishna S. A review on electrospinning design and nanofibre assemblies. Nanotechnology 2006;17:R89–106.
[27] Yang DY, Lu B, Zhao Y, Jiang XY. Fabrication of aligned fibrous arrays by magnetic electrospinning. Advanced Materials 2007;19:3702–6.
[28] Jin Y, Yang DY, Kang DY, Jiang XY. Fabrication of necklace-like structures via electrospinning. Langmuir 2010;26:1186–90.
[29] Zhang DM, Chang J. Patterning of electrospun fibers using electroconductive templates. Advanced Materials 2007;19:3664–7.

[30] Formhals A. Process and apparatus for preparing artificial threads. US patent No. 1975504; 1934.
[31] Reneker DH, Chun I. Nanometre diameter fibres of polymer, produced by electrospinning. Nanotechnology 1996;7:216–23.
[32] Lu XF, Bian XJ, Nie GD, Zhang CC, Wang C, Wei Y. Encapsulating conducting polypyrrole into electrospun TiO2 nanofibers: a new kind of nanoreactor for in situ loading Pd nanocatalysts towards p-nitrophenol hydrogenation. Journal of Materials Chemistry 2012;22:12723–30.
[33] Greiner A, Wendorff JH. Functional self-assembled nanofibers by electrospinning. Advances in Polymer Science 2008;219: 107–71.
[34] Schiffman JD, Schauer CL, Review: A. Electrospinning of biopolymer nanofibers and their applications. Polymer Reviews 2008;48:317–52.
[35] Agarwal S, Wendorff JH, Greiner A. Use of electrospinning technique for biomedical applications. Polymer 2008;49: 5603–21.
[36] Yang DY, Niu X, Liu YY, Wang Y, Gu X, Song LS, Zhao R, Ma LY, Shao YM, Jiang XY. Electrospun nanofibrous membranes: a novel solid substrate for microfluidic immunoassays for HIV. Advanced Materials 2008;20:4770–5.
[37] Yang DY, Liu X, Jin Y, Zhu Y, Zeng DD, Jiang XY, Ma HW. Electrospinning of poly(dimethylsiloxane)/poly(methylmethacrylate) nanofibrous membrane: fabrication and application in protein microarrays. Biomacromolecules 2009;10:3335–40.
[38] Chen W, He S, Pan WY, Jin Y, Zhang W, Jiang XY. A strategy for the modification of electrospun fibers that allows diverse functional groups for biomolecular entrapment. Chemistry of Materials 2010;22:6212–4.
[39] Liu Y, Sun Y, Yan H, Liu X, Zhang W, Wang Z, Jiang XY. Electrospun fiber template for replica molding of microtopographical neural growth guidance. Small 2012;8:676–81.
[40] Taylor G. Disintegration of water drops in an electric field. Proceedings of Royal Society of London Series A 1964;280:383–97.
[41] Taylor G, Electrically driven jets. Proceedings of Royal Society of London Series A 1969;313:453–75.
[42] Lukas D, Sarkar A, Pokorny P. Self-organization of jets in electrospinning from free liquid surface: A generalized approach. Journal of Applied Physics 2008;103, 084309/1-7.
[43] Reneker DH, Kataphinan W, Theron A, Zussman E, Yarin AL. Nanofiber garlands of polycaprolactone by electrospinning. Polymer 2002;43:6785–94.
[44] He JH, Wu Y, Zuo WW. Critical length of straight jet in electrospinning. Polymer 2005;46:12637–40.
[45] Reneker DH, Yarin AL, Fong H, Koombhongse S. Bending instability of electrically charged liquid jets of polymer solutions in electrospinning. Journal of Applied Physics 2000;87:4531–47.
[46] Yarin AL, Koombhongse S, Reneker DH. Bending instability in electrospinning of nanofibers. Journal of Applied Physics 2001;89:3018–26.
[47] Reneker DH, Yarin AL. Electrospinning jets and polymer nanofibers. Polymer 2008;49:2387–425.
[48] Shin YM, Hohman MM, Brenner MP, Rutledge GC. Electrospinning: A whipping fluid jet generates submicron polymer fibers. Applied Physics Letters 2001;78:1149–51.
[49] Shin YM, Hohman MM, Brenner MP, Rutledge GC. Experimental characterization of electrospinning: the electrically forced jet and instabilities. Polymer 2001;42:9955–67.
[50] Hohman MM, Shin M, Rutledge G, Brenner MP. Electrospinning and electrically forced jets. I. Stability theory. Physics of Fluids 2001;13:2201–20.
[51] Hohman MM, Shin M, Rutledge G, Brenner MP. Electrospinning and electrically forced jets. II. Applications. Physics of Fluids 2001;13:2221–36.
[52] Fridrikh SV, Yu JH, Brenner MP, Rutledge GC. Controlling the fiber diameter during electrospinning. Physical Review Letters 2003;90, 144502/1-4.
[53] Yarin AL, Kataphinan W, Reneker DH. Branching in electrospinning nanofibers. Journal of Applied Physics 2005;98, 064501/1-12.
[54] Huebner AL, Chu HN. Instability and breakup of charged liquid jets. Journal of Fluid Mechanics 1971;49:361–72.
[55] Fong H, Chun I, Reneker DH. Beaded nanofibers formed during electrospinning. Polymer 1999;40:4585–92.
[56] Tripatanasuwan S, Zhong ZX, Reneker DH. Effect of evaporation and solidification of the charged jet in electrospinning of poly(ethylene oxide) aqueous solution. Polymer 2007;48:5742–6.
[57] Han T, Reneker DH, Yarin AL. Buckling of jets in electrospinning. Polymer 2007;48:6064–79.
[58] Deitzel JM, Kleinmeyer J, Harris D, Beck Tan NC. The effect of processing variables on the morphology of electrospun nanofibers and textiles. Polymer 2001;42:261–72.
[59] Theron S, Zussman E, Yarin AL. Experimental investigation of the governing parameters in the electrospinning of polymer solutions. Polymer 2004;45:2017–30.
[60] Beachley V, Wen XJ. Effect of electrospinning parameters on the nanofiber diameter and length. Materials Science and Engineering: C 2009;29:663–8.
[61] Zheng J, Long YZ, Sun B, Zhang ZH, Shao F, Zhang HD, Zhang ZM, Huang JY. Polymer nanofibers prepared by low-voltage near-field electrospinning. Chinese Physics B 2012;21, 048102/1-6.
[62] Thompson CJ, Chase GG, Yarin AL, Reneker DH. Effects of parameters on nanofiber diameter determined from electrospinning model. Polymer 2007;48:6913–22.
[63] Katti DS, Robinson KW, Ko FK, Laurencin CT. Bioresorbable nanofiber-based systems for wound healing and drug delivery: optimization of fabrication parameters. Journal of Biomedical Materials Research Part B: Applied Biomaterials 2004;70:286–96.
[64] Zuo W, Zhu M, Yang W, Yu H, Chen Y, Zhang Y. Experimental study on relationship between jet instability and formation of beaded fibers during electrospinning. Polymer Engineering & Science 2005;45:704–9.
[65] Chase GG, Reneker DH. Nanofibers in filter media. Fluid/Particle Separation Journal 2004;16:105–17.
[66] Demir MM, Yilgor I, Yilgor E, Erman B. Electrospinning of polyurethane fibers. Polymer 2002;43:3303–9.
[67] Meechaisue C, Dubin R, Supaphol P, Hoven VP, Kohn J. Electrospun mat of tyrosine-derived polycarbonate fibers for potential use as tissue scaffolding material. Journal of Biomaterial Science, Polymer Edition 2006;17:1039–56.
[68] Zhang CX, Yuan XY, Wu LL, Han Y, Sheng J. Study on morphology of electrospun poly(vinyl alcohol) mats. European Polymer Journal 2005;41:423–32.
[69] Woodfield TBF, Van Blitterswijk CA, De Wijn J, Sims TJ, Hollander AP, Riesle J. Polymer scaffolds fabricated with pore-size gradients as a model for studying the zonal organization within tissue-engineered cartilage constructs. Tissue Engineering 2005;11:1297–311.
[70] Soliman S, Pagliari S, Rinaldi A, Forte G, Fiaccavento R, Pagliari F, Franzese O, Minieri M, Nardo PD, Licoccia S, Traversa E. Multiscale three-dimensional scaffolds for soft tissue engineering via multimodal electrospinning. Acta Biomaterialia 2010;6:1227–37.
[71] Pham QP, Sharma U, Mikos AG. Electrospun poly(ε-caprolactone) microfiber and multilayer nanofiber/microfiber scaffolds: characterization of scaffolds and measurement of cellular infiltration. Biomacromolecules 2006;7:2796–805.
[72] Han D, Gouma PI. Electrospun bioscaffolds that mimic the topology of extracellular matrix. Nanomedicine: Nanotechnology, Biology and Medicine 2006;2:37–41.
[73] Erisken C, Kalyon DM, Wang H. Functionally graded electrospun polycaprolactone and β-tricalcium phosphate nanocomposites for tissue engineering applications. Biomaterials 2008;29:4065–73.
[74] Shim IK, Jung MR, Kim KH, Seol YJ, Park YJ, Park WH, Lee SJ. Novel three-dimensional scaffolds of poly(L-lactic acid) microfibers using electrospinning and mechanical expansion: fabrication and bone regeneration. Journal of Biomedical Materials Research Part B: Applied Biomaterials 2010;95:150–60.
[75] Shim IK, Suh WH, Lee SY, Lee SH, Heo S, Lee MC, Lee SJ. Chitosan nano-/microfibrous double-layered membrane with rolled-up three-dimensional structures for chondrocyte cultivation. Journal of Biomedical Materials Research Part A 2009;90:595–602.
[76] Wang W, Itoh S, Matsuda A, Ichinose S, Shinomiya K, Hata Y, Tanaka J. Influences of mechanical properties and permeability on chitosan nano/microfiber mesh tubes as a scaffold for nerve regeneration. Journal of Biomedical Materials Research Part A 2008;84:557–66.
[77] Wang W, Itoh S, Konno K, Kikkawa T, Ichinose S, Sakai K, Ohkuma T, Watabe K. Effects of Schwann cell alignment along the oriented electrospun chitosan nanofibers on nerve regeneration. Journal of Biomedical Materials Research Part A 2009;91:994–1005.
[78] Cai YZ, Zhang GR, Wang L, Jiang YZ, Ouyang HW, Zou XH. Novel biodegradable three-dimensional macroporous scaffold using aligned electrospun nanofibrous yarns for bone tissue engineering. Journal of Biomedical Materials Research A 2012;100:1187–94.
[79] Leung LH, Khatounabad E, Naguib HE. Novel fabrication technique for 3-dimensional electrospun poly(DL-Lactide-Co-Glycolide) acid scaffolds. Proceedings of ASME/IMECE 2010;2:21–7.
[80] Leung LH, Fan S, Naguib HE. Fabrication of 3D electrospun structures from poly(lactide-co-glycolide acid)-nano-hydroxyapatite

composites. Journal of Polymer Science Part B: Polymer Physics 2011;50:242–9.
[81] Jenness NJ, Wu Y, Clark RL. Fabrication of three-dimensional electrospun microstructures using phase modulated femtosecond laser pulses. Materials Letters 2012;66:360–3.
[82] Lee BLP, Jeon H, Wang A, Yan Z, Yu J, Grigoropoulos C, Li S. Femtosecond laser ablation enhances cell infiltration into three-dimensional electrospun scaffolds. Acta Biomaterialia 2012;8:2648–58.
[83] Smit E, Büttner U, Sanderson RD. Continuous yarns from electrospun fibers. Polymer 2005;46:2419–23.
[84] Teo WE, Gopal R, Ramaseshan R, Fujihara K, Ramakrishna S. A dynamic liquid support system for continuous electrospun yarn fabrication. Polymer 2007;48:3400–5.
[85] Teo WE, Liao S, Chan CK, Ramakrishna S. Remodeling of three-dimensional hierarchically organized nanofibrous assemblies. Current Nanoscience 2008;4:361–9.
[86] Ki CS, Kim JW, Hyun JH, Lee KH, Hattori M, Rah DK, Park YH. Electrospun three-dimensional silk fibroin nanofibrous scaffold. Journal of Applied Polymer Science 2007;106:3922–8.
[87] Hong S, Kim GH. Fabrication of size-controlled three-dimensional structures consisting of electrohydrodynamically produced polycaprolactone micro/nanofibers. Applied Physics A 2011;103:1009–14.
[88] Gang EH, Ki CS, Kim JW, Lee J, Cha BG, Lee KH, Park YH. Highly porous three-dimensional poly(lactide-co-glycolide) (PLGA) microfibrous scaffold prepared by electrospinning method: a comparison study with other PLGA type scaffolds on its biological evaluation. Fibers and Polymers 2012;13:685–91.
[89] Yokoyama Y, Hattori S, Yoshikawa C, Yasuda Y, Koyama H, Takato T, Kobayashi H. Novel wet electrospinning system for fabrication of spongiform nanofiber 3-dimensional fabric. Materials Letters 2009;63:754–6.
[90] Kasuga T, Obata A, Maeda H, Ota Y, Yao X, Oribe K. Siloxane-poly(lactic acid)-vaterite composites with 3D cotton-like structure. Journal of Materials Science: Materials in Medicine 2012;23:2349–57.
[91] Zhang D, Chang J. Electrospinning of three-dimensional nanofibrous tubes with controllable architectures. Nano Letters 2008;8:3283–7.
[92] Chen F, Tang QL, Zhu YJ, Wang KW, Zhang ML, Zhai WY, Chang J. Hydroxyapatite nanorods/poly(vinyl pyrolidone) composite nanofibers, arrays and three-dimensional fabrics: Electrospun preparation and transformation to hydroxyapatite nanostructures. Acta Biomaterialia 2010;6:3013–20.
[93] Badrossamay MR, McIlwee HA, Goss JA, Parker KK. Nanofiber assembly by rotary jet-spinning. Nano Letters 2010;10:2257–61.
[94] Wang S, Zhang Y, Wang H, Yin G, Dong Z. Fabrication and properties of the electrospun polylactide/silk fibroin-gelatin composite tubular scaffold. Biomacromolecules 2009;10:2240–4.
[95] Zhou J, Cao C, Ma X. A novel three-dimensional tubular scaffold prepared from silk fibroin by electrospinning. International Journal of Biological Macromolecules 2009;45:504–10.
[96] Uttayarat P, Perets A, Li M, Pimton P, Stachelek SJ, Alferiev I, Composto RJ, Levy RJ, Lelkes PI. Micropatterning of three-dimensional electrospun polyurethane vascular grafts. Acta Biomaterialia 2010;6:4229–37.
[97] Wu H, Fan J, Chu CCh, Wu J. Electrospinning of small diameter 3-D nanofibrous tubular scaffolds with controllable nanofiber orientations for vascular grafts. Journal of Materials Science: Materials in Medicine 2010;21:3207–15.
[98] Subramanian A, Krishnan UM, Sethuraman S. Fabrication of uniaxially aligned 3D electrospun scaffolds for neural regeneration. Biomedical Materials 2011;6, 025004/1-10.
[99] Schneider OD, Weber F, Brunner TJ, Loher S, Ehrbar M, Schmidlin PR, Stark WJ. In vivo and in vitro evaluation of flexible, cottonwool-like nanocomposites as bone substitute material for complex defects. Acta Biomaterialia 2009;5:1775–84.
[100] Kim GH, Son JG, Park SA, Kim WD. Hybrid process for fabricating 3D hierarchical scaffolds combining rapid prototyping and electrospinning. Macromolecular Rapid Communications 2008;29:1577–81.
[101] Martins A, Chung S, Pedro AJ, Sousa RA, Marques AP, Reis RL, Neves NM. Hierarchical starch-based fibrous scaffold for bone tissue engineering applications. Journal of Tissue Engineering and Regenerative Medicine 2009;3:37–42.
[102] Moroni L, Schotel R, Hamann D, De Wjin JR, van Blitterswijk CA. 3D fiber-deposited electrospun integrated scaffolds enhance cartilage tissue formation. Advanced Functional Materials 2008;18:53–60.
[103] Park SH, Kim TG, Kim HC, Yang DY, Park TG. Development of dual scale scaffolds via direct polymer melt deposition and electrospinning for applications in tissue regeneration. Acta Biomaterialia 2008;4:1198–207.
[104] Kim SJ, Jang DH, Park WH, Min BM. Fabrication and characterization of 3-dimensional PLGA nanofiber/microfiber composite scaffolds. Polymer 2010;51:1320–7.
[105] Meng D, Erol M, Boccaccini AR. Processing technologies for 3D nanostructured tissue engineering scaffolds. Advanced Engineering Materials 2010;12:B467–87.
[106] Ji Y, Ghosh K, Shu XZ, Li B, Sokolov JC, Prestwich GD, Clark RAF, Rafailovich MH. Electrospun three-dimensional hyaluronic acid nanofibrous scaffolds. Biomaterials 2006;27:3782–92.
[107] Nam J, Huang Y, Agarwal S, Lannutti J. Improved cellular infiltration in electrospun fiber via engineered porosity. Tissue Engineering 2007;13:2249–57.
[108] Kim TG, Chung HJ, Park TG. Macroporous and nanofibrous hyaluronic acid/collagen hybrid scaffold fabricated by concurrent electrospinning and deposition/leaching of salt particles. Acta Biomaterialia 2008;4:1611–9.
[109] Leong MF, Rasheed MZ, Lim TC, Chian KS. In vitro cell infiltration and in vivo cell infiltration and vascularization in a fibrous, highly porous poly(D,L-lactide) scaffold fabricated by cryogenic electrospinning technique. Journal of Biomedical Materials Research Part A 2009;91:231–40.
[110] Simonet M, Schneider OD, Neuenschwander P, Stark WJ. Ultraporous 3D polymer meshes by low-temperature electrospinning: use of ice crystals as a removable void template. Polymer Engineering & Science 2007;47:2020–6.
[111] Widawski G, Rawiso M, Francois B. Self-organized honeycomb morphology of star-polymer polystyrene films. Nature 1994;369:387–9.
[112] Raez J, Manners I, Winnik MA. Nanotubes from the self-assembly of asymmetric crystalline-coil poly (ferrocenylsilane-siloxane) block copolymers. Journal of American Chemical Society 2002;124:10381–95.
[113] Ito Y, Virkar AA, Mannsfeld S, Oh JH, Toney M, Locklin J, Bao ZN. Crystalline ultrasmooth self-assembled monolayers of alkylsilanes for organic field-effect transistors. Journal of the American Chemical Society 2009;131:9396–404.
[114] Kalsin AM, Fialkowski M, Paszewski M, Smoukov SK, Bishop KM, Grzybowski BA. Electrostatic self-assembly of binary nanoparticle crystals with a diamond-like lattice. Science 2006;312:420–4.
[115] Bishop KJM, Wilmer CE, Soh S, Grzybowski BA. Nanoscale forces and their uses in self-assembly. Small 2009;5:1600–30.
[116] Yan G, Yu J, Qiu Y, Yi X, Lu J, Zhou X, Bai X. Self-assembly of electrospun polymer nanofibers: a general phenomenon generating honeycomb-patterned nanofibrous structures. Langmuir 2011;27:4285–9.
[117] Ma H, Hao J. Evaporation-induced ordered honeycomb structures of gold nanoparticles at the air/water interface. Chemistry-A European Journal 2010;16:655–60.
[118] Park MS, Kim JK. Broad-band antireflection coating at near-infrared wavelengths by a breath figure. Langmuir 2005;21:11404–8.
[119] Böker A, Lin Y, Chiapperini K, Horowitz R, Thompson M, Carreon V, Xu T, Abetz C, Skaff H, Dinsmore AD, Emrick T, Russell TP. Hierarchical nanoparticle assemblies formed by decorating breath figures. Nature Materials 2004;3:302–6.
[120] Lee SH, Park JS, Lim BK, Mo CB, Lee WJ, Lee JM, Hong SH, Kim SO. Highly entangled carbon nanotube scaffolds by self-organized aqueous droplets. Soft Matter 2009;5:2343–6.
[121] Connal LA, Vestberg R, Hawker CJ, Qiao GG. Fabrication of reversibly crosslinkable, 3-dimensionally conformal polymeric microstructures. Advanced Functional Materials 2008;18:3315–22.
[122] Connal LA, Qiao GG. Honeycomb coated particles: porous doughnuts, golf balls and hollow porous pockets. Soft Matter 2007;3:837–9.
[123] Zhang Y, Wang C. Micropatterning of proteins on 3D porous polymer film fabricated by using the breath-figure method. Advanced Materials 2007;19:913–6.
[124] Ma H, Hao J. Ordered patterns and structures via interfacial self-assembly: superlattices, honeycomb structures and coffee rings. Chemical Society Reviews 2011;40:5457–71.
[125] Thandavamoorthy S, Gopinath N, Ramkumar SS. Self-assembled honeycomb polyurethane nanofibers. Journal of Applied Polymer Science 2006;101:3121–4.
[126] Zhou FL, Gong RH. Manufacturing technologies of polymeric nanofibres and nanofibre yarns. Polymer International 2008;57:837–45.

[127] Baji A, Mai YW, Du X, Wong SC. Improved tensile strength and ferroelectric phase content of self-assembled polyvinylidene fluoride fiber yarns. Macromolecular Materials and Engineering 2012;297:209–13.
[128] Ko F, Gogotsi Y, Ali A, Naguib N, Ye HH, Yang GL, Li G, Willis P. Electrospinning of continuous carbon nanotube-filled nanofiber yarns. Advanced Materials 2003;15:1161–5.
[129] Wang X, Zhang K, Zhu M, Yu H, Zhou Z, Chen Y, Hsiao BS. Continuous polymer nanofiber yarns prepared by self-bundling electrospinning method. Polymer 2008;49:2755–61.
[130] Wang X, Zhang K, Zhu M, Hsiao BS, Chu B. Enhanced mechanical performance of self-bundled electrospun fiber yarns via post-treatments. Macromolecular Rapid Communications 2008;29:826–31.
[131] Penchev H, Paneva D, Manolova N, Rashkov I. Hybrid nanofibrous yarns based on N-carboxyethylchitosan and silver nanoparticles with antibacterial activity prepared by self-bundling electrospinning. Carbohydrate Research 2010;345:2374–80.
[132] Okuzaki H, Takahashi T, Miyajima N, Suzuki Y, Kuwabara T. Spontaneous formation of poly (p-phenylenevinylene) nanofiber yarns through electrospinning of a precursor. Macromolecules 2006;39:4276–8.
[133] Frenot A, Henriksson MW, Walkenström P. Electrospinning of cellulose-based nanofibers. Journal of Applied Polymer Science 2007;103:1473–82.
[134] Li MM, Long YZ. Fabrication of self-assembled three-dimensional fibrous stackings by electrospinning. Materials Science Forum 2011;688:95–101.
[135] Paneva D, Manolova N, Rashkov I, Penchev H, Mihai M, Dragan ES. Self-organization of fibers into yarns during electrospinning of polycation/polyanion polyelectrolyte pairs. Digest Journal of Nanomaterials & Biostructures 2010;5:811–9.
[136] Moon SC, Farris RJ. Strong electrospun nanometer-diameter polyacrylonitrile carbon fiber yarns. Carbon 2009;47:2829–39.
[137] Dalton AB, Collins S, Munoz E, Razal JM, Ebron VH, Ferraris JP, Coleman JN, Kim BG, Baughman RH. Super-tough carbon-nanotube fibres. Nature 2003;423:703.
[138] Khil MS, Bhattarai SR, Kim HY, Kim SZ, Lee KH. Novel fabricated matrix via electrospinning for tissue engineering. Journal of Biomedical Materials Research Part B: Applied Biomaterials 2005;72:117–24.
[139] Liu H, Leonas KK, Zhao Y. Antimicrobial properties and release profile of ampicillin from electrospun poly(ε-caprolactone) nanofiber yarns. Journal of Engineered Fibers & Fabrics 2010;5:10–9.
[140] Sun B, Long YZ, Yu F, Li MM, Zhang HD, Li WJ, Xu TX. Self-assembly of three-dimensional fibrous polymer sponge by electrospinning. Nanoscale 2012;4:2134–7.
[141] Bonino CA, menko KE, Jeong SI, Krebs MD, Alsberg E, Khan SA. Three-dimensional electrospun alginate nanofiber mats via tailored charge repulsions. Small 2012;8:1928–36.
[142] Brown TD, Dalton PD, Hutmacher DW. Direct writing by way of melt electrospinning. Advanced Materials 2011;23:5651–7.
[143] Lyons J, Li C, Ko F. Melt-electrospinning part I: processing parameters and geometric properties. Polymer 2004;45:7597–603.
[144] Luo CJ, Stoyanov SD, Stride E, Pelan E, Edirisinghe M. Electrospinning versus fibre production methods: from specifics to technological convergence. Chemical Society Reviews 2012;41:4708–35.
[145] Shabani I, Haddadi-Asl V, Seyedjafari E, Soleimani M. Cellular infiltration on nanofibrous scaffolds using a modified electrospinning technique. Biochemical and Biophysical Research Communications 2012;423:50–4.
[146] Vaz CM, Van Tuijl S, Bouten CVC, Baaijens FPT. Design of scaffolds for blood vessel tissue engineering. Acta Biomaterialia 2005;1:575–82.
[147] Soletti L, Hong Y, Guan J, Stankus JJ, El-Kurdi MS, Wagner WR, Vorp DA. A bilayered elastomeric scaffold for tissue engineering of small diameter vascular grafts. Acta Biomaterialia 2010;6:110–22.
[148] Szentivanyi A, Chakradeo T, Zernetsch H, Glasmacher B. Electrospun cellular microenvironments: Understanding controlled release and scaffold structure. Advanced Drug Delivery Reviews 2011;63:209–20.
[149] Vasita R, Katti DS. Nanofibers and their applications in tissue engineering. International Journal of Nanomedicine 2006;1:15–30.
[150] Han I, Shim KJ, Kim JY, Im SU, Sung YK, Kim M, Kang I, Kim JC. Effect of poly(3-hydroxybutyrate-*co*-3-hydroxyvalerate) nanofiber matrices cocultured with hair follicular epithelial and dermal cells for biological wound dressing. Artificial Organs 2007;31:801–8.
[151] Kumbar SG, Nukavarapu SP, James R, Nair LS, Laurencin CT. Electrospun poly(lactic acid-co-glycolic acid) scaffolds for skin tissue engineering. Biomaterials 2008;29:4100–7.
[152] Krishnan R, Rajeswari R, Venugopal J, Sundarrajan S, Sridhar R, Shayanti M, Ramakrishna S. Polysaccharide nanofibrous scaffolds as a model for in vitro skin tissue regeneration. Journal of Materials Science: Materials in Medicine 2012;23:1511–9.
[153] Kuppan P, Vasanthan KS, Sundaramurthi D, Krishnan UM, Sethuraman S. Development of poly(3-hydroxybutyrate-co-3-hydroxyvalerate) fibers for skin tissue engineering: effects of topography, mechanical, and chemical stimuli. Biomacromolecules 2011;12:3156–65.
[154] Zhu X, Cui W, Li X, Jin Y. Electrospun fibrous mats with high porosity as potential scaffolds for skin tissue engineering. Biomacromolecules 2008;9:1795–801.
[155] Jin G, Prabhakaran MP, Ramakrishna S. Stem cell differentiation to epidermal lineages on electrospun nanofibrous substrates for skin tissue engineering. Acta Biomaterialia 2011;7:3113–22.
[156] Powell HM, Supp DM, Boyce ST. Influence of electrospun collagen on wound contraction of engineered skin substitutes. Biomaterials 2008;29:834–43.
[157] Jin G, Prabhakaran MP, Kai D, Kotaki M, Ramakrishna S. Electrospun photosensitive nanofibers: potential for photocurrent therapy in skin regeneration. Photochemical & Photobiological Sciences 2013;12:124–34.
[158] Dimesso L, Spanheimer C, Jaegermann W, Zhang Y, Yarin AL. $LiFePO_4$-3D carbon nanofiber composites as cathode materials for Li-ions batteries. Journal of Applied Physics 2012;111, 064307/1-5.
[159] Krishnamoorthy T, Thavasi V, Subodh GM. Ramakrishna, A first report on the fabrication of vertically aligned anatase TiO2 nanowires by electrospinning: Preferred architecture for nanostructured solar cells. Energy & Environmental Science 2011;4:2807–12.
[160] Krishnamoorthy T, Tang MZ, Verma A, Nair AS, Pliszka D, Mhaisalkar SG, Ramakrishna S. A facile route to vertically aligned electrospun SnO2 nanowires on a transparent conducting oxide substrate for dye-sensitized solar cells. Journal of Materials Chemistry 2012;22:2166–72.
[161] Gibson P, Schreuder-Gibson H, Rivin D. Transport properties of porous membranes based on electrospun nanofibers. Colloids & Surfaces A: Physicochemical and Engineering Aspects 2011;187-188:469–81.
[162] Barhate RS, Ramakrishna S. Nanofibrous filtering media: Filtration problems and solutions from tiny materials. Journal of Membrane Science 2007;296:1–8.
[163] Zhang Q, Welch J, Park H, Wu C, Sigmund W, Marijnissen JCM. Improvement in nanofiber filtration by multiple thin layers of nanofiber mats. Journal of Aerosol Science 2010;41:230–6.
[164] Sambaer W, Zatloukal M, Kimmer D. 3D modeling of filtration process via polyurethane nanofiber based nonwoven filters prepared by electrospinning process. Chemical Engineering Science 2011;66:613–23.
[165] Wang W, Li Z, Jiang T, Zhao Z, Li Y, Wang Z, Wang C. Sulfonated poly(ether ether ketone)/polypyrrole core-shell nanofibers: A novel polymeric adsorbent/conducting polymer nanostructures for ultrasensitive gas sensors. ACS Applied Materials & Interfaces 2012;4:6080–4.
[166] Cavaliere S, Subianto S, Savych I, Jones DJ, Roziere J. Electrospinning: designed architectures for energy conversion and storage devices. Energy & Environmental Science 2011;4:4761–85.
[167] Persano L, Camposeo A, Tekmen C, Pisignano D. Industrial upscaling of electrospinning and applications of polymer nanofibers: A review. Macromolecular Materials & Engineering 2013;298:504–20.
[168] Sonina AN, Uspenskii SA, Vikhoreva GA, Filatov YN, Gal'braikh LS. Production of nanofibre materials from chitosan by electrospinning. Fibre Chemistry 2011;42:350–8.
[169] Chigome S, Torto N. A review of opportunities for electrospun nanofibers in analytical chemistry. Analytica Chimica Acta 2011;706:25–36.
[170] Nataraj SK, Yang KS, Aminabhavi M. Polyacrylonitrile-based nanofibers—A state-of-the-art review. Progress in Polymer Science 2012;37:487–513.
[171] Huang C, Soenen SJ, Rejman J, Lucas B, Braeckmans K, Demeester J, De Smedt SC. Stimuli-responsive electrospun fibers and their applications. Chemical Society Reviews 2011;40:2417–34.
[172] Zhong S, Zhang Y, Lim CT. Fabrication of large pores in electrospun nanofibrous scaffolds for cellular infiltration: A review. Tissue Engineering Part B: Reviews 2012;18:77–87.
[173] Wendorff JH, Agarwal S, Greiner A. Electrospinning: Materials, Processing and Applications. Weinheim, Germany: Wiley-VCH Verlag & Co KGaA; 2012. p. 256.

[174] Inagaki M, Yang Y, Kang F. Carbon nanofibers prepared via electrospinning. Advanced Materials 2012;24:2547–66.
[175] Lu XF, Zhang WJ, Wang C, Wen TC, Wei Y. One-dimensional conducting polymer nanocomposites: Synthesis, properties and applications. Progress in Polymer Science 2011;36:671–712.
[176] Niu HT, Wang XG, Lin T. Upward needleless electrospinning of nanofibers. Journal of Engineered Fibers & Fabrics 2012;7(3):17–22.
[177] Liu YQ, Zhang XP, Xia YN, Yang H. Magnetic-field-assisted electrospinning of aligned straight and wavy polymeric nanofibers. Advanced Materials 2010;22:2454–7.
[178] Petrick S, Maly M. Production nozzle-less electropspinning nanofibers technology www.elmarco.com/upload/soubory/dokumenty/66-1-1-mrs-fall-boston-09.pdf; 2009. 12 pp.
[179] Chang C, Limkrailassiri K, Lin L. Continuous near-field electrospinning for large area deposition of orderly nanofiber patterns. Applied Physics Letters 2008;93, 123111/1-3.
[180] Bisht GS, Canton G, Mirsepassi A, Kulinsky L, Oh S, Dunn-Rankin D, Madou MJ. Controlled continuous patterning of polymeric nanofibers on three-dimensional substrates using low-voltage near-field electrospinning. Nano Letters 2011;11:1831–7.
[181] Pu J, Yan X, Jiang Y, Chang C, Lin L. Piezoelectric actuation of direct-write electrospun fibers. Sensors & Actuators A: Physical 2010;164:131–6.
[182] Lee J, Jang J, Oh H, Jeong YH, Cho DW. Fabrication of a three-dimensional nanofibrous scaffold with lattice pores using direct-write electrospinning. Materials Letters 2013;93:397–400.
[183] Yoo HS, Kim TG, Park TG. Surface-functionalized electrospun nanofibers for tissue engineering and drug delivery. Advanced Drug Delivery Reviews 2009;61:1033–42.
[184] Ma Z, He W, Yong T, Ramakrishna S. Grafting of gelatin on electrospun poly(caprolactone) nanofibers to improve endothelial cell spreading and proliferation and to control cell orientation. Tissue Engineering 2005;11:1149–58.
[185] Kim TG, Park TG. Biomimicking extracellular matrix: cell adhesive RGD peptide modified electrospun poly(D,L-lactic-co-glycolic acid) nanofiber mesh. Tissue Engineering 2006;12:221–33.
[186] Shin YM, Shin H, Lim YM. Surface modification of electrosun poly(L-lactide-co -epsilon-caprolactone) fibrous meshes with a RGD peptide for the control of adhesion, proliferation and differentiation of the preosteoblastic cells. Macromolecular Research 2010;18:472–81.
[187] Casper CL, Yang W, Farach-Carson MC, Rabolt JF. Coating electrospun collagen and gelatin fibers with perlecan domain I for increased growth factor binding. Biomacromolecules 2007;8:1116–23.
[188] Park K, Ju YM, Son JS, Ahn KD, Han DK. Surface modification of biodegradable electrospun nanofiber scaffolds and their interaction with fibroblasts. Journal of Biomaterials Science, Polymer Edition 2007;18:369–82.
[189] Li WS, Guo Y, Wang H, Shi DJ, Liang CF, Ye ZP, Qing F, Gong J. Electrospun nanofibers immobilized with collagen for neural stem cells culture. Journal of Materials Science: Materials in Medicine 2008;19:847–54.
[190] Ku SH, Park CB. Human endothelial cell growth on mussel-inspired nanofibers scaffold for vascular tissue engineering. Biomaterials 2010;31:9431–7.
[191] Rim NG, Kim SJ, Shin YM, Jun I, Lim DW, Park JH, Shin H. Mussel-inspired surface modification of poly(L-lactide) electrospun fibers for modulation of osteogenic differentiation of human mesenchymal stem cells. Colloids & Surfaces B: Biointerfaces 2012;91:189–97.
[192] Zander NE, Orlicki JA, Rawlett AM, Beebe Jr TP. Quantification of protein incorporated into electrospun polycaprolactone tissue engineering scaffolds. ACS Applied Materials & Interfaces 2012;4:2074–81.
[193] Rim NG, Shin CS, Shin H. Current approaches to electrospun nanofibers for tissue engineering. Biomedical Materials 2013;8, 014102/1-14.
[194] Kim HW, Lee HH, Knowles JC. Electrospinning biomedical nanocomposite fibers of hydroxyapatite/poly(lactic acid) for bone regeneration. Journal of Biomedical Materials Research Part A 2006;79:643–9.
[195] Jeong SI, Ko EK, Yum J, Jung CH, Lee YM, Shin H. Nanofibrous poly(lactic acid)/hydroxyapatite composite scaffolds for guided tissue regeneration. Macromolecular Bioscience 2008;8:328–38.
[196] Lee JH, Lee YB, Rim NG, Jo SY, Lim YM, Shin H. Development and characterization of nanofibrous poly(lactic-co-glycolic acid)/biphasic calcium phosphate composite scaffolds for enhanced osteogenic differentiation. Macromolecular Research 2011;19:172–9.
[197] Sen R, Zhao B, Perea D, Itkis ME, Hu H, Love J, Bekyarova E, Haddon RC. Preparation of single-walled carbon nanotube reinforced polystyrene and polyurethane nanofibers and membranes by electrospinning. Nano Letters 2004;4:459–64.
[198] Leung V, Ko F. Biomedical applications of nanofibers. Polymers for Advanced Technologies 2011;22:350–65.